BRNO UNIVERSITY OF TECHNOLOGY

Faculty of Electrical Engineering
and Communication

MASTER'S THESIS

Brno, 2020 Bc. Radovan Juráň

BRNO UNIVERSITY OF TECHNOLOGY

VYSOKÉ UČENÍ TECHNICKÉ V BRNĚ

FACULTY OF ELECTRICAL ENGINEERING AND COMMUNICATION

FAKULTA ELEKTROTECHNIKY
A KOMUNIKAČNÍCH TECHNOLOGIÍ

DEPARTMENT OF RADIOENGINEERING

ÚSTAV RADIOELEKTRONIKY

FIELD SENSOR NETWORK FOR MICROCLIMATOLOGICAL MEASUREMENTS

TERÉNNÍ SENZOROVÁ SÍŤ PRO MIKROKLIMATOLOGICKÁ MĚŘENÍ

MASTER'S THESIS
DIPLOMOVÁ PRÁCE

AUTHOR — **Bc. Radovan Juráň**
AUTOR PRÁCE

SUPERVISOR — **Ing. Aleš Povalač, Ph.D.**
VEDOUCÍ PRÁCE

BRNO 2020

BRNO UNIVERSITY OF TECHNOLOGY
FACULTY OF ELECTRICAL ENGINEERING AND COMMUNICATION

Master's Thesis

Master's study field **Electronics and Communication**

Department of Radioengineering

Student: Bc. Radovan Juráň ***ID:*** 165411

Year of study: 2 ***Academic year:*** 2019/20

TITLE OF THESIS:

Field sensor network for microclimatological measurements

INSTRUCTION:

Define sensor network requirements for measuring and monitoring selected environmental parameters (CO2 concentration, humidity, temperature) in the Hranice Karst area. The system will include battery-powered metering stations with optimized energy consumption, which will send data to the concentrator via LPWAN communication (e.g. LoRaWAN). Design a block concept and create a prototype device that will read and send data.

Design a complete schematic diagram, PCB and hardware solution optimized for outdoor environment. Assemble the device and verify its functionality. Process and visualize the measured data in an appropriate way.

RECOMMENDED LITERATURE:

[1] GERLACH, Gerald, Ulrich GUTH a Wolfram OELSSNER, ed. Carbon Dioxide Sensing: Fundamentals, Principles, and Applications. Weinheim, Germany: Wiley-VCH Verlag GmbH & Co., 2019. ISBN 978-3-5-7-41182-5.

[2] About the LoRaWAN® Specification [online]. [cit. 2020-01-26]. Dostupné z: https://lora-alliance.org/lorawa--for-developers

Date of project specification: 3.2.2020 ***Deadline for submission:*** 28.5.2020

Supervisor: Ing. Aleš Povalač, Ph.D.
Consultant: doc. Mgr. Milan Geršl, Ph.D., Mendlova univerzita

prof. Ing. Tomáš Kratochvíl, Ph.D.
Subject Council chairman

ABSTRACT

This work is focused on the design of a field wireless sensor network for microclimatological measurements, especially juvenile carbon dioxide emissions in the area of hydrothermal karst, based on LoRaWAN. The theoretical part of the thesis presents an overview of the target location, possible solutions for measuring, obtaining and transmitting data. The practical part is then devoted to the complete design of the entire system – from the measuring device through the concentrator and gateway to the backend of sending data to the cloud storage. The results of this complex problem are presented continuously and the appendices contain more detailed and illustrative examples.

KEYWORDS

LoRa, LPWAN, LoRaWAN, carbon dioxide, CO2, IoT, low-power, hydrothermal karst, microclima

ABSTRAKT

Tato práce je zaměřena na návrh terénní bezdrátové senzorové sítě pro mikroklimatologická měření, zejména výronů juvenilního oxidu uhličitho v oblasti hydrotermílního krasu, založené na LoRaWAN. V teoretické části práce je předložen přehled cílové oblasti, možností řešení měření, získávání a přenosu dat. Praktická část se pak věnuje kompletnímu návrhu celého systému, to znamená od měřicího zařízení přes koncentrátor a gateway až po backend odesílání dat do cloudového úložiště. Výsledky tohoto komplexního problému jsou prezentovány průběžně a přílohy obsahují detailnější a názornější ukázky.

KLÍČOVÁ SLOVA

LoRa, LPWAN, LoRaWAN, oxid uhličitý, CO2, IoT, low-power, hydrotermální kras, mikroklima

JURÁŇ, Radovan. *Field sensor network for microclimatological measurements*. Brno, Rok, 91 p. Master's Thesis. Brno University of Technology, Faculty of Electrical Engineering and Communication, Department of Radio Electronics. Advised by Ing. Aleš Povalač, Ph.D.

Rozšířený abstrakt diplomové práce

V souladu s článkem 3 odst. 7 a článkem 15 odst. 5 Směrnice č. 72/2017 Vysokého učení technického v Brně je tato práce, předkládaná v anglickém jazyce, uvedena rozšířeným abstraktem v jazyce českém. Tato část práce obsahuje nečíslované a necitované stránky, počínaje touto, které obsahují úvod do problematiky, nástin řešení a zhodnocení výsledků.

Úvod

Tato práce pojednává o kompletním návrhu terénní bezdrátové měřicí sítě, určené ke sledování charakteristických parametrů mikroklimatu hydrotermálního krasu. Konkrétně se jedná o sledování výronů juvenilního oxidu uhličitého v Hranickém krase, k nimž dochází ve zdejších jeskyních, v řece Bečvě i ve volné krajině. Právě místa v otevřené krajině, kde plyn vystupuje ze země (tzv. *ventaroly* neboli *mastné fleky*), jsou vhodné k jeho sledování. Tyto výrony jsou spojené s polohou tohoto území, kde dochází ke hlubinnému styku geomorfologických celků Českého masivu a Karpat. Tento proces se podílel i na vzniku zdejší minerální vody, teplické kyselky, která je balneologicky využívána už od 16. století zdejšími lázněmi v Teplicích nad Bečvou. Kyselka je také důležitým činitelem formování Zbrašovských aragonitových jeskyní a Hranické propasti, nejhlubší zatopené sladkovodní propasti světa.

Cílem práce je kompletní návrh celého systému měření od infrastruktury LPWAN bezdrátové sítě po jednotlivé měřicí stanice.

Řešení

Bezdrátová síť LPWAN

Bezdrátová síť byla postavena na LoRaWAN. Jádrem je gateway připojená k internetu, která prostřednictvím komunitních bezplatných služeb The Things Network předává data přijatá z LoRaWAN na on-line úložiště dat (v době testování zařízení byly jako úložiště využity Tabulky Google s privátním přístupem vázaným na Účet Google majitele dané tabulky). Gateway se sestává z mikropočítače Raspberry Pi 3 B+, koncentrátoru IMST iC880a a propojovací desky, navržené a vyrobené na míru v rámci této práce. Propojovací deska umožňuje signálové i mechanické propojení použitého hardware. Obstarává také napájení celé gateway integrovaným stejnosměrným měničem Mean Well SCW12A-05, který dovoluje napájet desku vstupním

v rozmezí stejnosměrného napětí +9 až +18 V (jmenovitě +12 V) s pevným výstupem +5 V pro Raspberry i koncentrátor. Napěťové úrovně jsou indikovány LED. Použitá 3 dBi anténa pro kmitočet 868 MHz je připojena pigtailovanou redukcí mezi IPX konektorem koncentrátoru a SMA.

Aby bylo možné ověřit, že zvolená infrastruktura bezdrátové sítě obsáhne sledovanou lokalitu, bylo provedeno jednoduché měření intenzity přijatého signálu pomocí RSSI (Received Signal Strength Indication), o němž dává informaci samotná gateway s každým příchozím rámcem dat. Data byla vysílána z několika vybraných míst v blízkosti sledovaných ventarol a obsahovala přímo zeměpisné souřadnice ve formátu WGS84, získané lokalizací mobilního telefonu. Takto získané uspořádané trojice dat byly následně vyneseny do mapy a interpolovány v geografickém informačním systému QGIS. Vzhledem k charakteru krajiny údolí řeky Bečvy v oblasti měření lze předpokládat chování přenosového kanálu rámcově za dobře odhadnutelné.

Měřicí stanice jako uzly LPWAN sítě

Měřicí stanice jsou bateriově napájené, a tedy návrh směřuje k vytvoření zařízení s relativně nízkou spotřebou. S tímto ohledem byly pro návrh hardware stanic zvoleny takové součástky, které tento záměr podporují. Napájení je z baterie snižováno na úroveň +5 V a +3,3 V dvěma spínanými měniči Texas Instruments LM63625. Řidicím členem je MCU (mikrokontrolér) STM32L010RB v pouzdře LQFP64 z řady orientované na nízkou spotřebu (low-power zařízení), který je napájen +3,3V větví a ovládá veškeré periferie, včetně povolování +5V větve, k níž jsou připojena čidla, pro úsporu energie v případě jejího nepoužívání. Komunikační člen, umožňující připojit zařízení do sítě LoRaWAN je Microchip RN2483, ovládaný příkazy přes UART. Čidla je možné připojit samostatně do svorkovnic, které obsahují dostupné datové sběrnice nebo analogové vstupy pro A/D převod veličin z ryze anaglových čidel. Návrh počítá zejména s variabilitou čidel CO_2 , kdy je možnost připojit buď Wisen MH-Z16 (UART) nebo Sensirion SCD-30 (I2C), v závislostina zvolené kombinaci propojek nulových rezitorů. MCU řídí kromě zmíněných periferií a čidel také homogenizační ventilátor, který je umístěný v jímací komoře na CO_2 . Jímací komora je sestavena z odpadní KG přesuvky průměru 250 mm s plexisklovým víkem, otevíratelným stejnosměrným motorem regulovaným PWM (pulse width modulation, pulzně šířková modulace) pro odvětrání komory. Principem je totiž hromadění plynu v jímací komoře na základě rozdílu koncetrací plynu v půdě a vzduchu. Sledovaným parametrem je nárůst koncentrace CO_2 v čase, z něhož ze známých rozměrů komory lze stanovit tok plynu v čase. Tyto měřicí stanice jsou uzly (*nodes*) LoRaWAN sítě.

Zhodnocení výsledků a závěr

Výsledkem práce je kompletní návrh bateriově napájeného zařízení, které slouží k obsluze jímací komory plynu oxidu uhličitého, vyčítání dat z čidel a odesílání těchto dat směrem k gateway LoRaWAN sítě. Samotná gateway sestavená v rámci této práce částečně z hotového hardware a doplněná vlastními návrhy, přeposílá tato data do databáze umístěné na internetu prostřednictvím služeb The Things Network. V době testování sítě byly jako úložiště zvoleny Tabulky Google. Toto uložení dat posloužilo i k terénnímu experimentu se silou vysílaného singálu LoRa z modulu RN2483. Vznikla tak infrastruktura, která umožní budoucí rozšíření i o sběr dat z jiných měření, včetně vylepšení měření stávajícího.

DECLARATION

I declare that I have written the Master's Thesis titled "Field sensor network for microclimatological measurements" independently, under the guidance of the advisor and using exclusively the technical references and other sources of information cited in the thesis and listed in the comprehensive bibliography at the end of the thesis.

As the author I furthermore declare that, with respect to the creation of this Master's Thesis, I have not infringed any copyright or violated anyone's personal and/or ownership rights. In this context, I am fully aware of the consequences of breaking Regulation § 11 of the Copyright Act No. 121/2000 Coll. of the Czech Republic, as amended, and of any breach of rights related to intellectual property or introduced within amendments to relevant Acts such as the Intellectual Property Act or the Criminal Code, Act No. 40/2009 Coll., Section 2, Head VI, Part 4.

Brno ....

author's signature

ACKNOWLEDGEMENT

I would like to thank Ing. Aleš Povalač, Ph.D. for mentoring, consultation, patience and suggestive ideas. Likewise, I would like to thank the expert consultant doc. Mgr. Milan Geršl, Ph.D. for experienced advice in the field of target application.

Brno . . . .

author's signature

Faculty of Electrical Engineering
and Communication
Brno University of Technology
Purkynova 118, CZ-61200 Brno
Czech Republic
http://www.six.feec.vutbr.cz

ACKNOWLEDGEMENT

Research described in this Master's Thesis has been implemented in the laboratories supported by the SIX project; reg. no. CZ.1.05/2.1.00/03.0072, operational program Výzkum a vývoj pro inovace.

Brno ....
author's signature

EVROPSKÁ UNIE
EVROPSKÝ FOND PRO REGIONÁLNÍ ROZVOJ
INVESTICE DO VAŠÍ BUDOUCNOSTI

Contents

List of Figures

List of Tables

Introduction

Measuring microclimatological parameters of the environment is a complex, interdisciplinary problem. Especially when it comes to a long-term, large-scale and multi-site field measurements, where conventional manual collection of samples might become a time consuming, laborious, and ineffective process.

Long-term measuring of any physical quantity is nowadays easier thanks to various methods of autonomous digital data acquisition. On top of that, recent boom of the Internet of Things (IoT) has brought to use several robust, long-range, yet still low-power and relatively affordable means of wireless communication, minimizing the need of human intervention. This enables to combine conventional data loggers *in situ* with wireless data transmissions over relatively long distance directly to an end device, which collects these data and either stores them or passes to a cloud server for further processing.

This work is dedicated to designing a whole system of field sensor network for microclimatological measuremetns based on LPWAN (Low Power Wide Area Netwok), which will be deployed and tested in area of hydrothermal karst. To understand the measured phenomena, the first part of this thesis briefly indtroduces the target area of deployment – the hydrothermal karst – and explains basic mechanisms and origin of the measured phenomena. The second part describes theoretical assumptions in terms of used methods, technologies and compares possible solutions. Also a brief introduction of selected LPWAN is presented in the second part. The third part brings detailed description and justification of decisions made in the design process based upon the theory. Fourth part gives an overview of achieved results, which are then summarized in the Conclusion.

This masters thesis shall bring two main outcomes – fristly provide a better way to deepen current understanding of complex processes in hydrothermal karst and secondly asseses IoT means of wireless data transmission performance in an open terrain. Both of these goals shall be achieved by using the equipment designed in this work according to individual points of this master's thesis assignment.

1 Locality

The system designed in this master's thesis is primarily intended to be tested and fully deployed to conduct measurements in the locality of Hranice Karst. The system's main goal is to measure microclimatological parameters typical for this hydrothermal karst area with main focus on carbon dioxide (CO_2) degassing. To understand where this CO_2 comes form and what exactly is the subject of measurement of this thesis, this chapter brings a brief overview of local geological conditions given by complicated development of this area.

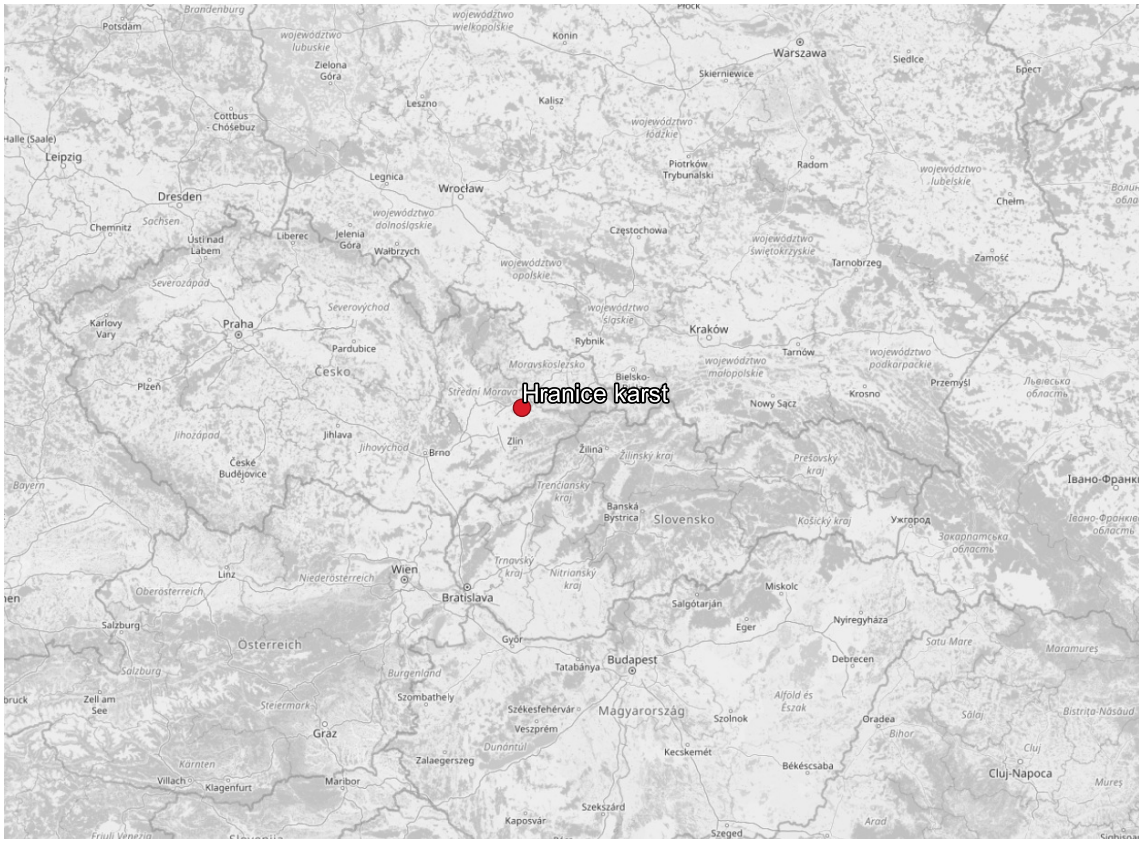

Fig. 1.1: Location of Hranice Karst, viewed with QGIS on openstreetmap.org map data 1:4500000 scale (author)

Hranice Karst is a unique area of hydrothermal karst located in Moravia, eastern Czech Republic. Besides Zbrašov Aragonite Caves (ZAC), the Hranice Abbys is located in this territory, being considered the deepest flooded cave in the world with so far measured depth of 473,5 m, with the bottom still undiscovered by this day. From geological point of view, the Hranice Karst is based on devonian limestones on the border of Bohemian Massif and Western Carpathians. Briefly stated, the contact of these two geomorphological units caused an opening of old, deep structures, allowing juvenile carbon dioxide to rise from depths of Earth's mantle along these

cracks towards the surface. The CO_2 dissolves in meteoric water, creating mineral water, which then not only significantly formed the Hranice Karst, but is also being used in local spa of Teplice nad Bečvou.[10]

Fig. 1.2: Example of observable carbon dioxide outflow in the Bečva River (author)

The carbon dioxide degassing is not only observable both in Hranice Abbys and Zbrašov Aragonite Caves, but also in the water of river Bečva and even in an open land, too. These places in terrain are called *ventaroles* (latin *ventus*, wind) and can be best seen during winter, as the CO_2 is relatively warm and melts nearby snow. These vetaroles are the measuring sites for the designed system, as the main goal is to map the surface CO_2 flux in the area. Measuring sites are described in detail in chapters below.

2 Theoretical Analysis

The previous chapter described the main physical phenomena – CO_2 and its natural outflow from ground in a specific area – as the subject of the measurement. A successful design of a device capable of measuring CO_2 flux must be based on a detailed summary of current experience, knowledge and experiments conducted in this filed so far. This chapter introduces an overview of several publications on this topic and brings summarized information, which shall serve as basic requirements for developed device and whole system.

2.1 Concentration

One of the fundamental terms used in this work is concentration. In a qualitative way, concentration is the amount of one particular substance that is found within another substance. Concentration c is usually used with mixtures, being considered as an amount or a number of entities n per a defined volume V of the mixture:

$$c = \frac{n}{V} 100\ [\%] \tag{2.1}$$

Concentration – as any ratio – can be also be expressed as a percentage 2.1, speaking of a part of the whole as a part of 100, but for lower concentrations unit *ppm* (parts per milion) is usually used 2.2:

$$100\,\% = 1000000\,ppm \tag{2.2}$$

2.2 Flux

In general, the amount of a property transported across a surface per unit time is a quantity called the flux. There are more expressions of fluxes, such as volumetric, mass flux, etc. depending on the property observed.[11] As a scalar, flux through given area A can be defined as follows:

$$J = \frac{I}{A}, \tag{2.3}$$

where

$$I = \lim_{x \to \infty} \frac{\Delta q}{\Delta t} = \frac{dq}{dt}, \tag{2.4}$$

where J is a general flux, q observed quantinty and t time.

2.3 Soil carbon dioxide flux

Besides the geologial processes which take place under ground, soil is a source of CO_2 production itself as a sum of many subsources – respiration of microorganisms, plant roots and organic material decomposition etc. Therefore there is usually a steep gradient between CO_2 concentration in the soil compared to that in the ambient air. This creates a diffusive exhange between the upper soil layers and the atmosphere near the soil surface, which is the main driving force of the soil CO_2 flux (in other words the CO_2 transport). The efflux is also partialy supported by pressure changes generated by moving air above soil.[12, 13]

This diffusion-driven flux corresponds to Fick's first law of diffusion:

$$J_A = -D_{AB}\frac{d\varphi}{dx}, \tag{2.5}$$

where J_A is the diffusion flux (amount of substance per unit area per unit time; see flux above 2.3), D is the *diffusion coefficient* or *diffusivity* (area per unit time) and φ is the concentration (amount of substance per unit volume; see 2.1), and x is position (distance).[14]

To have the theory complete, let's mention that there's also been defined the Second Fick's law [14], which predicts the concentration change in time for one dimension as follows:

$$\frac{d\varphi}{dt} = D\frac{d\varphi^2}{dx^2}, \tag{2.6}$$

2.4 Soil carbon dioxide flux measurements

Measurements of soil gas fluxes of varoius sources have been conducted for nearly one century all over the world across science disciplines. The first scientist who measured soil respiration in the field was Henrik Lundegårdh in 1927.[12] Since then, an extensive research has been conducted to develop a variety of measurement methods. Yet still, even according to many scientists, it is reasonable to admit that accurate measurement of soil gases fluxes is an extraordinarily challenging task, as there are many both primary and secondary influences on both the measurement and CO_2 efflux itself, which shall be taken in account at least to some extent.[13] In connection with that, it shall be stated that this work is focused on pursuing the precision and repeatability in observing continuous, long-term dynamic changes rather than the accuracy of each one particular measurement.

As with any measurement, there are several methods for conducting the measurement of the soil-surface carbon dioxide fluxes. In terms of used method the techniques can be divided in absorption-based, gasometric (chamber), gradient and micrometeorolgical. The chamber gasomtetric methos are further devided into dynamic and static. Yet none of these techniques is considered as preferable, as each has its own advantages and disadvantages, as well as susceptibilitiy to measurement errors.

2.4.1 Absorption Methods

These methods are based on chemical reactions, using a sorbet that is able to bind CO_2 from the measured air. The CO_2 flux is the calculated from difference in mass of the sorbent before and after the measuring. Nowadays these methods are not used anymore and have been replaced by more accurate methods.[12, 13]

2.4.2 Chamber (Gasometric) Methods

The most used techniques for CO_2 soil flux measurement are chamber-based methods, which provide measurements of efflux directly from the soil surface. Chamber methos can be divided into open, where the air leaves the system, and closed, where the measured air is held in the chamber. Both are mainly based on CO_2 mainly infrared gas analysers (IRGA).

Chamber methods are in general relatively non–expensive and easy to operate, making them adaptable for a wide variety of applications. So far most of the published measuring results were backed only either by commercial or DIY unstandardised systems. On the other hand, a universal standardisatised chamber system – either commercial or DIY – does not exist [13].

Open chamber

In an open (steady-state, flow-through) system, there's a chamber covering an area of soil, through which the air stream is constantly flowing and as it passes through the chamber, it gets enriched by a certain ammount of the measured gas. The gas concentration is measured before the air enters the chamber and taken as a reference to be compared against concentration upon leaving the chamber. Flux F_{CO_2} is then computed as the difference of these two concentrations times the flow rate of the system divided by the area coverd by chamber 2.7:

$$F_{CO_2} = \frac{1}{R}\frac{Pv}{AT}(C_{Reference} - C_{Sample}), \tag{2.7}$$

where:

- F_{CO_2} – the CO_2 flux $[\mu mol\, m^{-2}\, s^{-1}]$,

- R – molar gas constant [8.314 $Pa\ m^3\ K^{-1}\ mol^{-1}$],
- P – atmospheric pressure [Pa],
- v – air flow through the chamber [$m^3\ s^{-1}$],
- A – area of the soil covered by the chamber [m^3],
- T – air temperature [K],
- C_2 – CO_2 concentration after leaving the system [ppm],
- C_1 – CO_2 concentration upon entering the system [ppm],

There are non-negligible disadvantages, such as limited sensitivity due to using two gas analysers and the measurement accuracy depends on how well are they matched one to another, as any differences can easily cause false readings and distortion. The air-flow applied has to be known precisely for the computation and in addition a high flow rate can create pressure differential. Another disadvantage is inherent harming the natural environmental conditions in general – the chamber covers the soil and remains closed for a long period of time, which affects natural conditions.

Closed chamber

On the other hand, in the closed chamber (transient, non-steady-state) method the chamber is fully enclosed and there is no gas exchange with ambient air. The CO_2 flux is estimated from the CO_2 concentration increase inside the chamber over time. 2.8

$$F_{CO_2} = \frac{PV}{RT}\frac{dC}{dt}A^{-1}, \tag{2.8}$$

where:

- P –atmospheric pressure,
- V – chamber's volume [m^3],
- dC/dt – the change of the chamber CO_2 concentration in time [μmol/mol/s],
- R – molar gas constant [8.314 $Pa\ m^3/K/mol$]
- A – covered soil area [m^2].

Since most of the commercial as well as home-made chamber systems used for gas flux measurements are based on the closed dynamic approach, the closed chamber method was chosen as the method of measurement for this work too, as there is enough experience in this field which makes it also easier to evaluate in the future. It is described in detail in the next part of the text.

2.5 Closed chamber automated system

In 2018, a working group of the pan-european long-term research infrastructure Integrated Carbon Observation System (ICOS) decided to set standards and quality checks for chamber systems in order to define minimum requirements for the chamber measurement systems. [13] These are summarized here chapter and serve as one of the main sources of information for this work.

A typical chamber system for gas measurements consists of these parts:

- the chamber itself,
- a collar inserted into the ground onto which the chamber is secured,
- a sampling unit and a gas analyser,
- a controlling unit to operate the chamber system,
- storage for the measurement data.

These points can be illustrated with a block scheme depicted on figure 2.1, which brings a better overview.

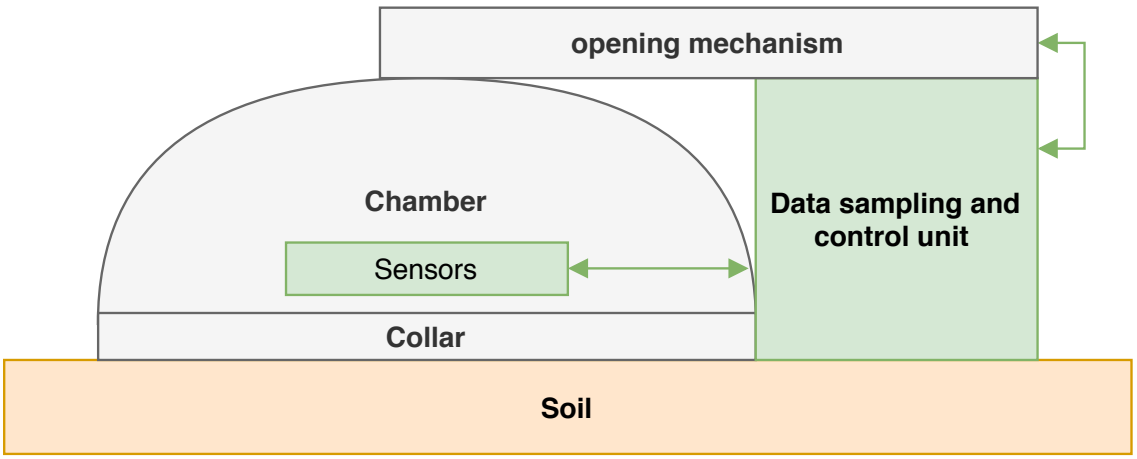

Fig. 2.1: General block diagram of a common system (author)

These points mentioned above have a close relationship to the most important considerations for an accurate measurement:

- maintaining the chamber-pressure equilibrium with ambient air pressure,
- ensuring good mixing of the air inside the chamber,
- dealing with an altered diffusion gradient inside the chamber,
- minimizing the disturbance to the environment.

2.5.1 Chamber design requirements

As ICOS states, is almost impossible to define a standard chamber. This part of text summarizes available experience both from commercial and empiric sources;

all cited.

Usually the system relies on an external gas analyser. These are usually connected via inlet tubes (pipes or hoses) located around the half of the chamber height are fitted with a net or filter to avoid insects incoming to the measurement system. This work aims to reduce the price for an external analyser, using the CO_2 sensor directly in the chamber.

Chamber shape is one of the thing that affects mixing. Although any chamber shape is acceptable, assessing required homogeneity in the chamber as critical parameter makes cylindrical shape best choice, as it allows better mixing of the inside air. When it comes to chamber volume, it plays a significant role to choose good ration between area covered by the chamber, volume of the chamber, time spend filling the chamber with gas, as well as being able to ventilate it. The volume depends on rates measured, because doubling the volume will cut the change in CO_2 concentration in a half. (source:licor) In addition, the larger the chamber, the more the signal measured becomes diluted. If the chamber is too large, the signal is on par with the background noise of the analyser.

Material of chamber is important for many reasons. Firstly, choosing opaque material instead of transparent can reduce increasing of temperature in head-space of the chamber. Secondly, some materials are more water-repelling and shall be preferred, because humidity of air inside the chamber can form water drops on the inside walls, resulting in relatively longer time needed for the chamber to stabilize. Lastly, some materials can absorb CO_2 , therefore inert and non-permeable materials are recommended by ICOS, among which these examples are enlisted:

- Polyvinylchloride (PVC),
- Polypropylene (PP),
- Polyethylene (PE),
- Acrylonitrile-Butadiesen-Styrene (ABS),
- Polytetrafluoroethylene (PTFETeflon),
- Polymethyl Methacrylate (PMMA),
- stainless steel,
- aluminium.

2.5.2 Pressure equilibrium

To accurately represent the flow rate occurring naturally outside the chamber it is required to maintain a balanced pressure between the inside of the chamber and outside air, therefore chambers shall be fitted with a vent in order to avoid pressure changes when closing and opening the chambers, but also during the measurement.

There are many ways to observe this condition, but one mechanism must be taken

in account especially – the Bernoulli's principle and Venturi effect. The Bernoulli's principle described by equation 2.10 bellow states that an increase in the speed of a fluid occurs simultaneously with a decrease in static pressure or a decrease in the fluid's potential energy.**??**

$$P_1 + \frac{1}{2}\rho v_1^2 + \rho g h_1 = P_2 + \frac{1}{2}\rho v_2^2 + \rho g h_2, \tag{2.9}$$

where:

- $P_{1,2}$ – the pressures,
- ρ – the density of the medium,
- $v_{1,2}$ – medium velocities,
- $h_{1,2}$ – the elevations,
- g – the gravitational acceleration.

From the Bernoulli's principle description of the Venturi effect can be derrived, representing reduction in fluid pressure that results when a fluid flows through a constricted section (or choke) of a pipe [15]:

$$P_1 - P_2 = \frac{\rho}{2}(v_2^2 - v_1^2) \tag{2.10}$$

This principles are important when considering wind conditions, because as wind passes over the vent tube's external open end, it causes changes both in pressure and speed in time. Therefore using a simple vent tube can be effective only under calm wind conditions. This rises the flow of CO_2 –rich air from the soil into the chamber, leading to a significant overestimation of CO_2 flux. A special patented vent was designed [1] for these purposes in commercially available devices, based on principles described above.

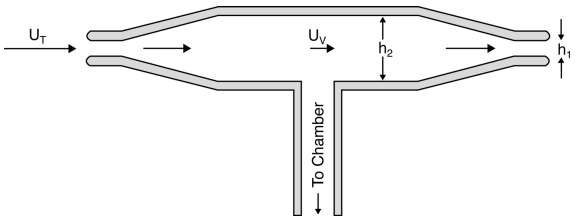

Fig. 2.2: Cross-section view of the radially symmetric commercial vent design, adopted from [1]

The vent shape assumes, that conservation of mass requires that the average air flow rate drops as the air enters the vent. This design is radially symmetric to eliminate wind-direction sensitivity.

2.5.3 Mixing of the air inside the chamber

The air inside the chamber headspace is needed to be homogenous, because only a small portion of it's volume is evaluated by gas analyser and it needs to be a representative sample. In a well mixed chamber, gas concentrations are homogenous throughout the chamber, because turbulence is such that no pockets of still air develop.

Although chamber shape helps the air homogenization, it needs to be supported to achieve air movement similar to the outside wind speed close to ground surface. The most of commercial systems rely on airflow between the chamber and gas analyser. Also, a fan installed in the chamber can be used for mixing. However, this can have a slight drawback – rotating fan too much can cause disturbances in the pressure equilibrium and disrupt the high laminar boundary layer above the soil. Rotation regulation of the fan is the key to cope with this problem.

2.5.4 Altered diffusion gradient inside the chamber

Soil CO_2 flux is driven primarily by the CO_2 diffusion gradient across the soil surface. On the other hand, the CO_2 concentration must be allowed to rise in order to obtain dC/dt. However, raising concentration will reduce the diffusion gradient across the soil surface inside the chamber, leading to an underestimation of the flux.

This problem shall be taken in account when representing the results measured. In some literature, linear functions are fit to measured data, but it doesn't take in account these changes. This has been overcame by an exponential function derived to fit the measured data. With the initial slope of the fitted function, the flux is then estimated at the time when CO_2 concentration is close to the ambient level.

$$C_{CO_2} = C_S + \left[C_{CO_2}(0) - C_S\right] e^{-at} \tag{2.11}$$

$$\frac{dC_{CO_2}}{dt} = a\left[C_S - C_{CO_2}(0)\right] e^{-at} \tag{2.12}$$

where C_S is the CO_2 concentration in the soil surface layer communicating with the chamber, and a is a rate constant.

2.5.5 Collar

The collar ensures stability of the chamber and its insertion to soil should assure a good airtight chamber-to-soil seal. Soil collars for automated chamber measurements should consist of materials similar to those used on chamber. Although the optimal collar design depends on the ecosystem type, shape and size of collar should

minimize disturbances to the soil surface and its insertion should be as shallow as possible. Higher porosity requires deeper insertion.

After the installation of the soil collars measurements of GHG can be started. Acquired data has to be analysed for effects of collar insertion (disturbance) in measured fluxes on the base of principal investigator (PI) experience.

2.6 Sensor instrumentation and auxiliary measurements

Reducing influence on the environment is important, because the overall accuracy of the measurements is based on environmental conditions and if possible not harming them. Especially for long-time measurements it is necessary to keep conditions in the chamber and around it as natural as possible to minimize any unwanted influence on the results.

Some commercially available chambers are constructed with these specific needs in mind. These systems are usually placed on a perforated baseplate, which minimizes the perturbation to the soil environment around the chamber collar. The chamber itself is removable and able to be automatically parked away from its collar when not conducting any measurement. This helps to eliminate any possibility of pushing too much fresh air into the soil or removing soil air during the chamber moving. Temperature effects are compensated by used materials and coatings.

Fig. 2.3: Example of a commercially available measurement unit Li-Cor 8100, adopted from [2]

Therefore it requires several parameters to be taken in consideration. The fundamental requirement for an accurate CO_2 flux measurement is that the deployment

of measuring apparatus must have no or minimal impact on disturbance to environment conditions that have influence on soil CO_2 production and transport across the soil surface and that these conditions are monitored along with the flux to understand measured data better.

Attention should be paid to changes of the microclimate inside the chamber compared to climate conditions around the chamber. Therefore, besides compensation of the measuring apparatus presence several auxiliary measurements of additional parameters should be part of the system as well. There are several variables to be observed and the chamber should be instrumented with sensors for measuring them in intervals coordinated with the sampling of the gas analysers.

2.6.1 Gas analyser

Gas analyser is one of the most important things. There are a few parameters to be considered when selecting the right one. Firstly, the short-term stability, in other words the drift in baseline concentrations over a short timescale. The measurement range has to cover all presumed (anticipated) concentrations of the measured gas in the target environment, but it is relative to the time of chamber closure and its size. ICOS recommends the range of at least 100 – 2000 ppm with sampling frequency at least 0.1 Hz for CO_2 . There are several types of CO_2 sensors, based upon different physical principles, some of which are described in the chapter which discusses selected hardware.

2.6.2 Ventilation

As the gas concentration rises, it reaches point at which diffusion can't continue naturally. It is recommended to keep a minimum closure time of 5 min to ensure that even very low fluxes can be measured accurately. Again, this procedure can be managed by various means, however with the demand for a long-time measurement in mind, there is a need to make the air exchange process as effective as possible, yet still with a good seal when re-closed, while keeping it not so much energy demanding.

2.6.3 Soil and air temperature

As stated in the flux equation 2.8, temperature fluctuations during measurement are necessary in the process of flux calculations. The sensor should be protected from direct sun light and positioned not too close to the walls or lid to prevent biased values due to surface heating of chamber material.

Soil temperature is to be measured inside the chamber. The depth of these measurements depends on the type of ecosystem and soil. However, following the compulsory measurement depths of soil temperature in the upper soil layer, one measurement at 5 cm is mandatory and one measurement as close to the soil surface as possible is optional.

2.6.4 Soil moisture

A soil water content sensor should be installed close to each collar when a small chamber is used or inside of big chambers. The measurement depth should be close to the soil surface (5 cm) for CO_2 and following the sensor manufacturer recommendations.

2.7 Measuring Sites

The measuring sites were selected both from those where measurements had already taken place in the past and those yet to be observed.The previous measurements provide an estimate for the required measuring range of the sensors and the possibility of comparison of the results.

Tab. 2.1: Measuring sites, coordinates in WGS 84 format, data from JESO and mobile positioning by Mapy.cz (author)

Name	**N**	**E**
Rozvrt	49°31'39.288"	17°44'43.692"
Půlhodina	49°31'55.200"	17°44'58.020"
U rybízu	49°31'55,2"	17°44'58,4"

All these sites 2.1 are in the vicinity of Zbrašov aragonite caves administration building, as seen on figure 2.4. As there is electricity and internet connection, it makes it a prefect location for placing a data concentrator and utilzing the concept of lowpower wide area network described further.

2.8 Data acquisition

2.8.1 In-situ data storage

Most devices for long-term field measurement use data storage located *in situ*, e.g. in the device using some kind of dedicated storages hardware, such as flash memory

Fig. 2.4: Measuring sites and Zbrašov aragonite caves administration building shown on map, created in QGIS with openstreetmap.org map data (author)

or SD card. This is a reliable method, but has a major drawback – the data are accessible only when collected manually from the device and if the device is broken or the measurement is not going on properly for any reason, it might be discovered days or hours after the measurement is started. Therefore, firstly any data loses are not detected and secondly any faults of the measurement processes are not known until data are examined.

Of course hard data storage is a perfect redundancy, but problem described above can be overcome by a wireless transfer, where even if signal loss can occur time to time, data can be stored away from the field, preferably on a cloud server. This approach not only helps to protect data, but also speeds up their analysis.

2.8.2 Wireless data transmissions

Although measuring devices are in general application specific, in most cases such a device is battery powered and located in relatively faraway location, which makes manual data collecting a demanding activity. In addition, even if the battery or data storage capacity would suffice in most cases for a long period of time, any

malfunction might occur and jeopardize the whole process without any noticing by causing data losses or even stopping the whole measuring.

Putting some of available definitions together, it can be stated, that the way of extending the interconnection via the Internet beyond standard devices by traditionally noninternetenabled physical devices by means of various technologies is called collectively by an abstract term Internet of Things (IoT). Because the Internet itself is a network by its nature, IoT is based on networks too. One type of a network utilized in IoT, is called Low Power Wide-Area Network (LPWAN).

2.8.3 LoRa and LoRaWAN

LoRa physical layer

LPWAN is primarily intended to interconnect devices, that send small amounts of data in longer time periods over long distances among various environments without a human interaction. One of these networks is called LoRaWAN and run on LoRa physical layer.

Fig. 2.5: Logo of LoRa, adopted from [3]

LoRa is a registered trademark technology, which introduces the physical layer for creating a long range, bi-directional communication link with low power characteristics and robustness to interference. A complete description of the LoRa physical layer is provided by Semtech in their LoRa Modulation Basics manual [16]. Yet to understand efficiency and philosophy of LoRa physical layer, at least basics shall be illustrated.

Generally, the base of LoRa is a spread spectrum modulation, which is a technique that intentionally spreads narrow band signals over a much wider band, so

the entire bandwidth is used for the transmission. This is used in many communication systems, because a narrow band signal is easily interfered or jammed and more power is needed to overcome this problem. The spread spectrum utilizes the same power, but spreads out the power density while maintaining the same or better link budget. The resulting low–power, noise–like signals make the transmitted signal harder to interfere with and to get detected. The spreading itself is achieved in a classic Direct Sequence Spread Spectrum (DSSS) by multiplying the data with a pseudorandom noise-like sequence (chips) of higher rate in the transmitter. This brings another advantage – the data get encoded. Then, the receiver re-multiplies the received signal again with the same chips, and gets the original data.[16, 17, 18, 19]

Besides DSSS, there are more methods, like Frequency Hopping Spread Spectrum (FHSS) or, utilized in LoRa, Chirp Spread Spectrum (CSS). The CSS uses a chirp signal, which is continuously changing frequency over time. This combines spread spectrum and frequency–shift keying techniques. The bandwidth is scalable, allowing either shorter distance and higher bandwidth link, or vice versa. Data rate is adaptive according to selected bandwidth. This approach eliminates multipath echoes and Doppler–shift. Reduced interference reduces the need to re–transmit data, which also lessens power requirements, making it fit for battery-powered devices. Also, as no synchronization is needed, the system is less complex, thus low in price, and again reduces the power needs.[16, 17, 18, 19]

Standardization

LoRa is a physical layer for an open standard LPWAN called LoRaWAN. Standardisation and the accredited certification scheme of LoRaWAN to maintain interoperability is maintained by LoRa Alliance, a non-profit association of companies. It defines the communication protocol for the network on which LoRa operates (and for which provides the physical layer). The LoRaWAN specification [3] states, that networks are usually star–of–stars, in which gateways (concentrators, base stations) transmit messages between end–devices (motes) and a central Network Server, which routes the packets from each device to associated Application Server. Security of LoRaWAN relies on symmetric cryptography using session keys derived from root keys of the device. Gateway use standard IP, end devices use the above previously described LoRa mechanisms. The communication is bi-directional, although uplink from the end–device is considered a dominant traffic. Further, the document summarizes LoRa spreading spectrum mechanisms and trade–offs between range and data rate described in the physical layer details above. [3]

LoRaWAN recognizes 3 device Classes, of which at least A–capability must be implemented and compatibility ensured. Class A allow the lowest power, bi-

Application				
LoRa MAC				
Class A (baseline)		*Class B (beacon)*	*Class C (continuous)*	
LoRa Modulation				
Regional ISM band				
EU 868	*EU 433*	*US 915*	*AS 430*	*...*

Tab. 2.2: LoRaWAN Classes and layers, adopted from [3]

directional device–driven communications. Only after a uplink there are two short downlink receive windows. Class B opens extra downlink windows at scheduled times. Class C have continuously open receive windows except for when uplink takes place, therefore latency is low, but energy consumption the highest.

Region	Europe	North America
Frequency Band	867-869 MHz	902-928 MHz
Channels	10	64+8+8
Bandwidth Up	125/250 kHz	125/500 kHz
Bandwidth Dn	125 kHz	500 kHz
TX Power Up	14 dBm	14 dBm
TX Power Dn	20 dBm (30 dBm allowed)	27 dBm
Spreading factor	7-12	7-10
Data rate	250bps-50kbps	980bps-21.9kpbs

Tab. 2.3: LoRaWAN summary, adopted from [3]

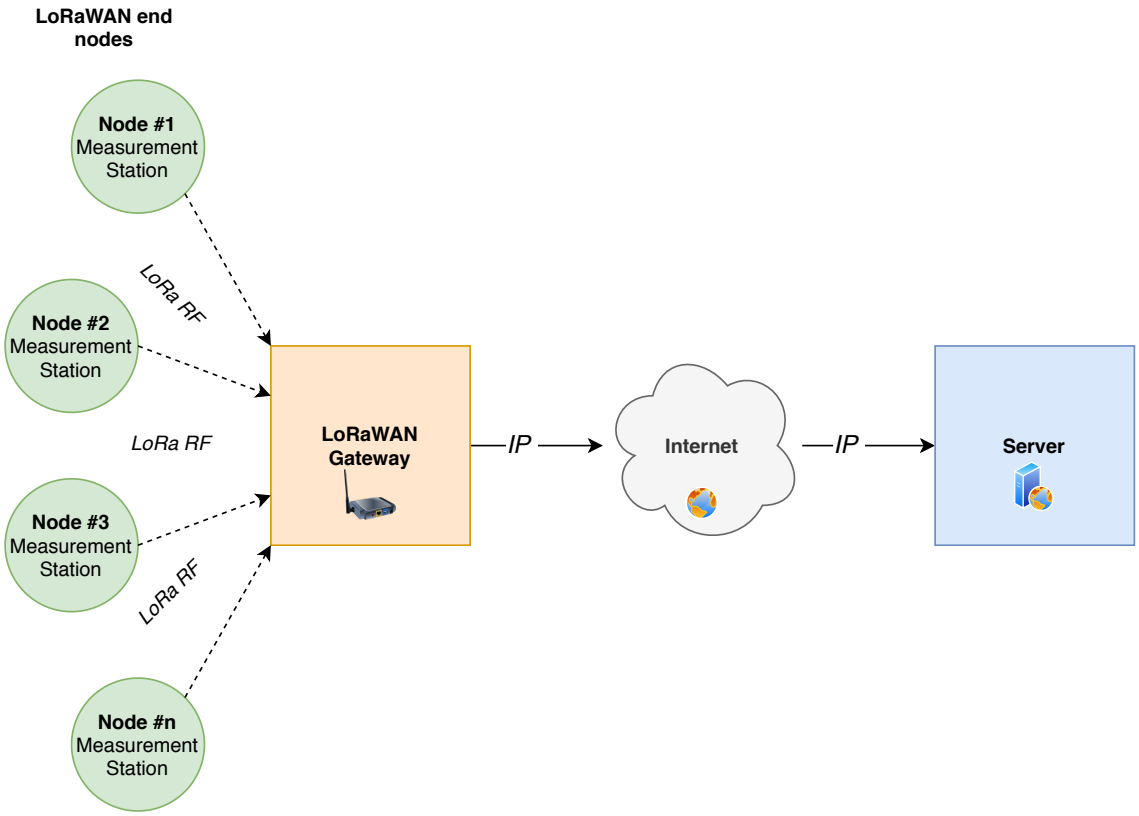

Fig. 2.6: General block diagram of a common system (author)

3 Selecting Elements of Implementation

The previous chapter presented theoretical assumptions and requirements on the designed system, which are then used in this chapter to choose the means to solve the problems stated. First of all, an overall block scheme of the whole system is presented, as seen of figure 4.1. Individual parts of the system are then further described in detail in each their own separate subchapters, assesing their attributes, properties and abilities to fit the designed system as a whole.

3.1 Chamber, collar and ventilation

The aim was to find a way to obtain a chamber easy to use and relatively low in price. For this purpose a waste pipe was selected, because it combines inexpensivity, robust stability when placed on ground to withstand gusts of wind, ability to be used with another waste pipe conuterparts as chamber collars or lids, and therefore has vast flexibility in use.

3.2 Mixing fan

The mixing fan should be regulatable to change rotation speed, because localized pressure gradients could develop or the soil surface could get excessively ventilated. [20] At first, using a standard 2-pin DC computer fan without any regulation was considered together with designing an own regulator unit for it. Due to availability of off-the-shelf pulse width modulation (PWM) regulated fans sold for personal computers at fair prices, it was decided to use these.

3.3 Sensors

Selection of sensors was driven not only by a trade-off between their sparametrs and price, but there was also the third important parameter to consider – overall resistance to climatic conditions in the chamber (rain, temperautre changes, etc.)

3.3.1 CO_2 Sensor

Because measuring the CO_2 concentration gradient is the most important part of the whole measurement set, three candidates were chosen to be compared and put to test.

MG811

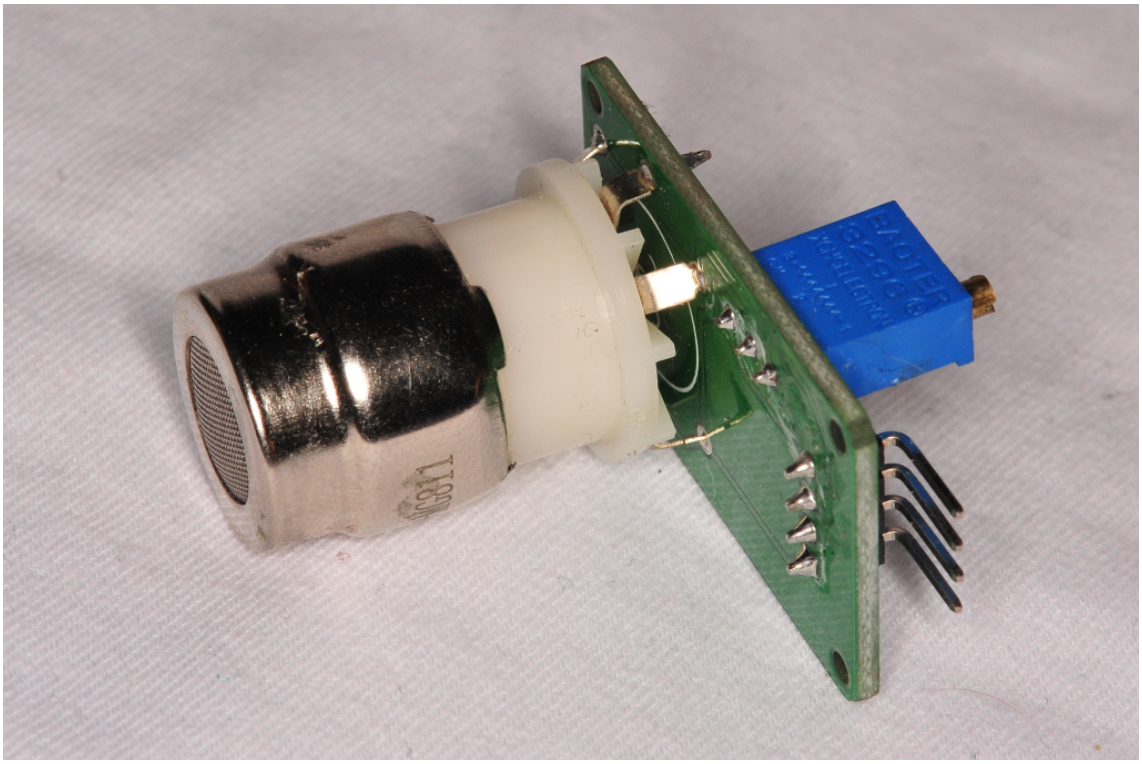

Fig. 3.1: Photo of the MG811 sensor, purchased for evaluation (author)

The MG811 is based on the direct measurement with solid electrolyte cells principle and chemical reactions which take palce on the used electrodes. [21, 4] It offers analog output proportional to 350-10000 ppm range. Yet still, a callibration process would be needed, as only the analog value is available as the output.[21]

The electrodes have to be preheated by DC current, requiring power 1200 mW at +6 V to operate properly, giving need of 200 mA current. The use of AC current is allowed too.[21] This is a major drawback of this sensor, because even if assuming turning the sensor on and off to save power during its inactivity, this fact indicates inappropriate energy requirements and therefore is unsuitable for this low power and energy saving oriented application. Another drawback of this sensor is the absence of any cover or box from the manufacturer that would protect the electronics from the effects of the environment, however, this could be solved by installing the sensor in a separate box with a cable gland.

SCD30

This sensor by Sensirion combines ability to evaluate CO_2 concentration, air humidity, and temperature at once, which makes it a very versatile option that covers most

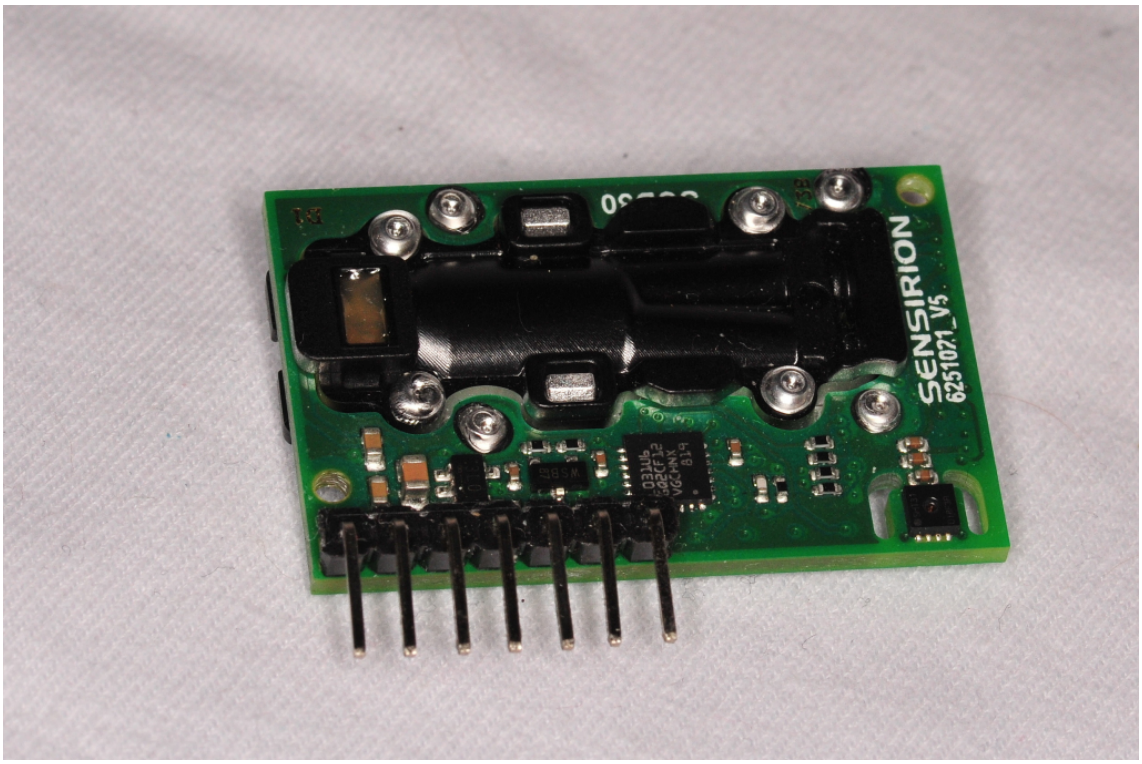

Fig. 3.2: Photo of the SCD30 sensor, purchased for evaluation (author)

of the needs defined in the theoretical analysis of this work. With its parameters, it supports efforts to design a low-power circuit and is also sufficient and suitable for the application in terms of accuracy and speed of measuring changes in all measured quantities. The worst case current draw is 75 mA in voltage range form +3.3 to +5.5 V, which brings incomparable difference copared to MG811. The CO_2 measuring is calibrated, linearized and temperature compesated internally. The output is either UART/Modbus, I2C bus for all the digital data available or PWM output (pulse width proportional solely to CO_2 concentration). Available range of measurable CO_2 concentration is 400–10000 ppm and offers the ability to be calibrated. [22]

The gas concentraion measuring part of the sensor utilizes analytical method of detection based on nondispersive infra-red spectroscopy (NDIR).[22] It utilizes principle of concentration-dependent absorption of infrared part of electromagnetic specrum range by the measured gas molecules. Therefore, only the transmission of wavelengths which correspond to characteristic absorption bands of the gases to be detected takes place and can be recorded, so the method can be also called single-wavelength specrophotometer. For CO_2 these wavelengths are around 4.24 μm.[4]

The Lambert–Beer law states that light absorption depends on both the path

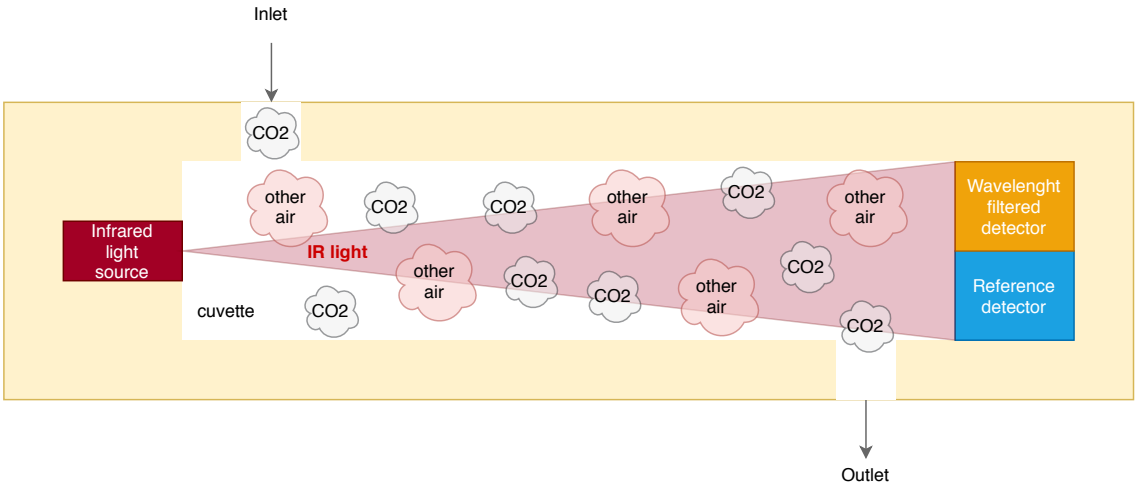

Fig. 3.3: Principle of NDIR method based sensors (author, by description in literature [4])

length-dependent attenuation of the intensity I during passage through the absorbing gas and the gas concentration C.[4]

$$I_1 = I_0 + e^{\epsilon C d}, \tag{3.1}$$

where I_1 is the intensity in 4.24 μm band channel, I_0 intensity of reference channel, $\epsilon(\lambda)$ is the extinction or absorption coefficient, C gas concentraion and d is the distance between light source and detectors. The reference detector compensates for the effect of fluctuations in the intensity of the light source, therefore when the intensity changes, the ratio of I_0 and I_1 will remain unchanged. From this it can be derrived by comparing measured intesinty of the lightsource and intensity measured in deisred filtered part of the spectrum according to the Lambert-Beer law, concentration is equal to:

$$C = \ln(\frac{I_1}{I_0})\frac{1}{\epsilon d} \tag{3.2}$$

There is a major drawback – absence of any cover leaving the sensor electronics exposed to the environment, as in this case any casing would affect directly the parameters measured.

MH-Z16

This is an to previsous sensor made by Winsen, which does not have the capability to measure temperature and air humidity, but offers quite robust waterproof casing for its electronics on the other hand. This sensor is also temperature compensated, linearized, and offers the ability to be calibrated. It operates from 4.5 V to 5.5 V

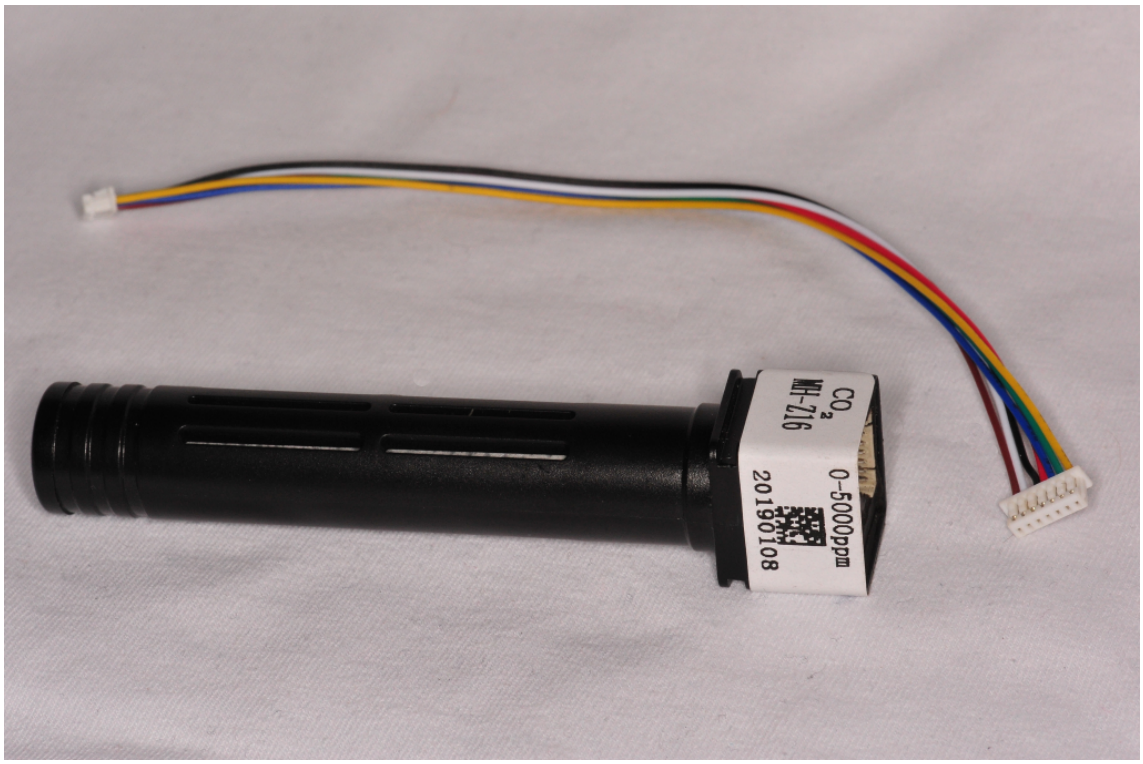

Fig. 3.4: Photo of the MHZ16 sensor, purchased for evaluation (author)

drawing 85 mA in the worst case. There are more variants of measurement range available at the market, but the selected and evaluated version offered 0-5000 ppm. Output of the sensor is versatile – UART, PWM or analog value.

The drawback is only one quantity measured compared to SCD30. Because of that, additional sensors are needed to be picked as a suitable and cost efficient alternative.

Comparison of the CO_2 sensors

To compare the sensors purchased for testing, an experiment was performed, which shows the response of the sensors to the conditions of changes in the measured quantity to which it will be exposed during the actual measurement. Each sensor was wired and powered according its respective datasheet provided by the manufacturer.

The x-axis represents time in hh:mm:ss format, while the y-axis shows measured CO_2 concentration in parts per milion change in time. The course of the experiment is identical to the principle of operation of the gas chamber. It took place in a bedroom, where a certain concentration of the measured gas was already present. A few moments after starting the measurement, the room was intensively ventilated by opening the windows. Subsequently, the room was closed again and used for its purpose. In the morning, the ventilation and closing of the windows was repeated.

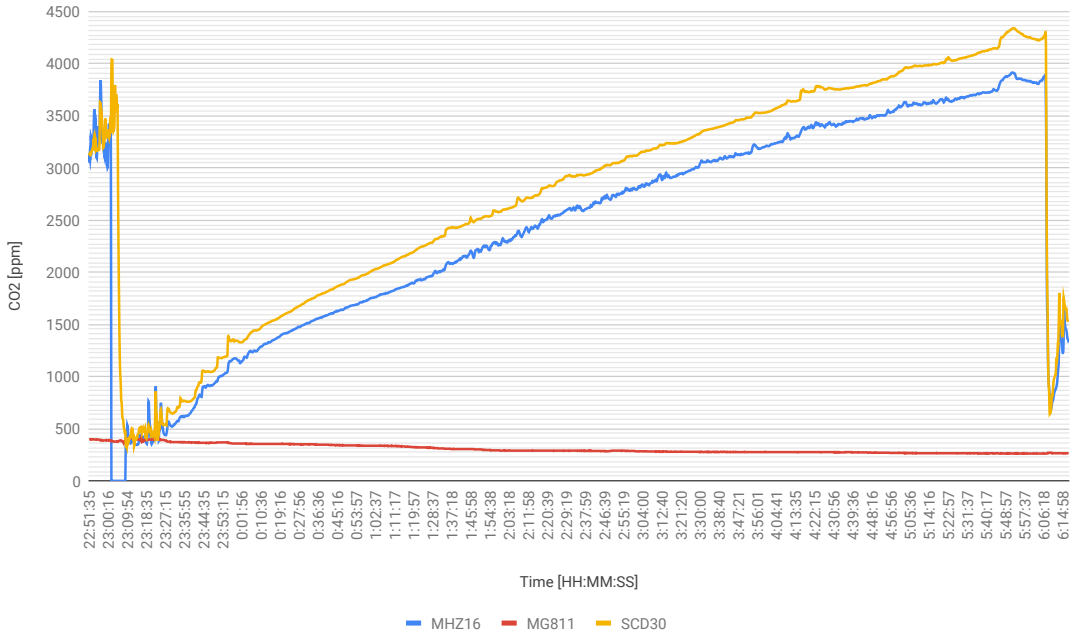

Fig. 3.5: Comparison of the evaluated sensors (author)

The gasometric gas chamber works on the same principle. By looking at the trends of presented curves, the SCD30 and MHZ16 performed simillarily, but MG811 was irresponsive.

3.3.2 Soil and Air Temperature

Digital 1-Wire bus waterproof DS18B20 thermometer was chosen to measure temperature of both air and soil. It is capable of measuring temperatures from $-55°C$ to $125°C$ with accuracy $\pm 0.5°C$ in range from $-10°C$ to $85°C$, which is sufficient during normal climatic conditions throughout the year in central Europe. Digital output of the thermometer has programmable resolution (9 up to 12 bits) proportional to conversion time and can be directly represented on the Celsius scale.

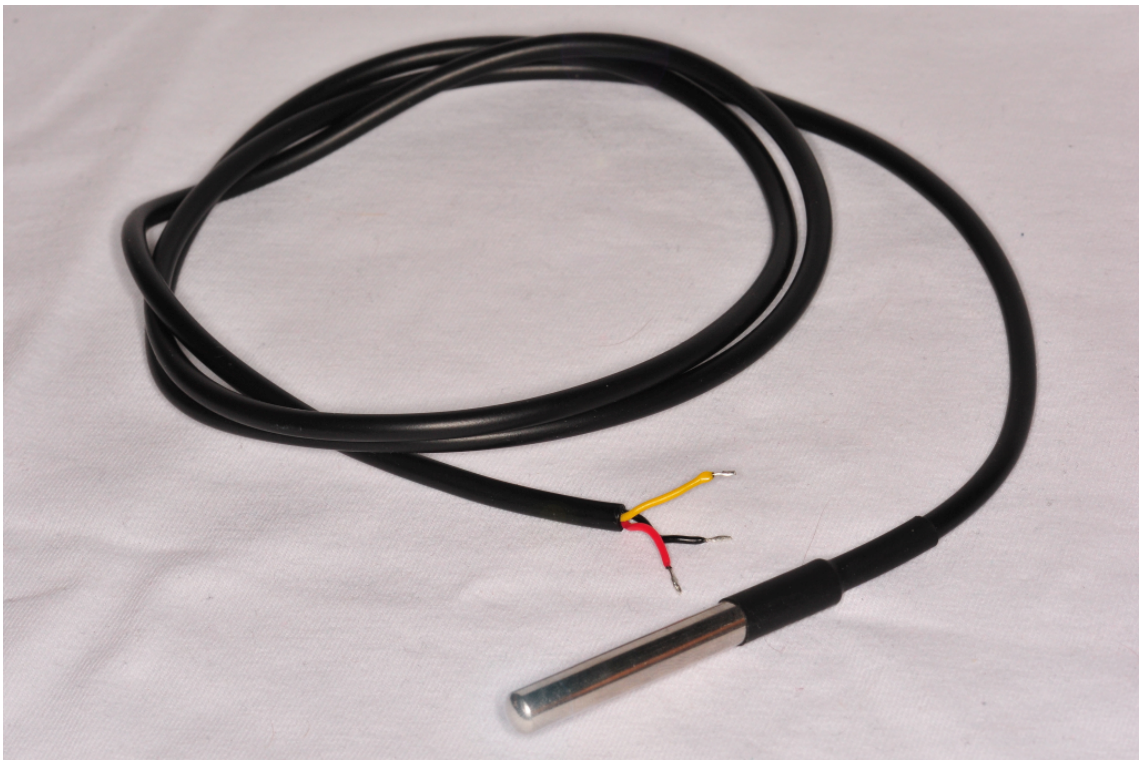

Fig. 3.6: Photo of the DS18B20 digital waterproof temperature sensor, purchased for evaluation (author)

3.3.3 Soil Moisture

The simpliest capacitive soil moisture sensor on market was chosen. Although it has a bare, unprotected PCB, the price overweights this drawback. The principle of this sensor is based on the principle of operation of the capacitor. The dielectric consists of water and ions dissolved in it. A change in humidity changes the dielectric, a change in dielectric changes the capacity. The change in capacitance is measured by a circuit based on a circuit 555, at the output of which the voltage changes precisely depending on the capacitance of the capacitor, formed by the sensor electrodes and moist soil. This voltage can be then converted to digital value, the range of which can be represented as moisture.

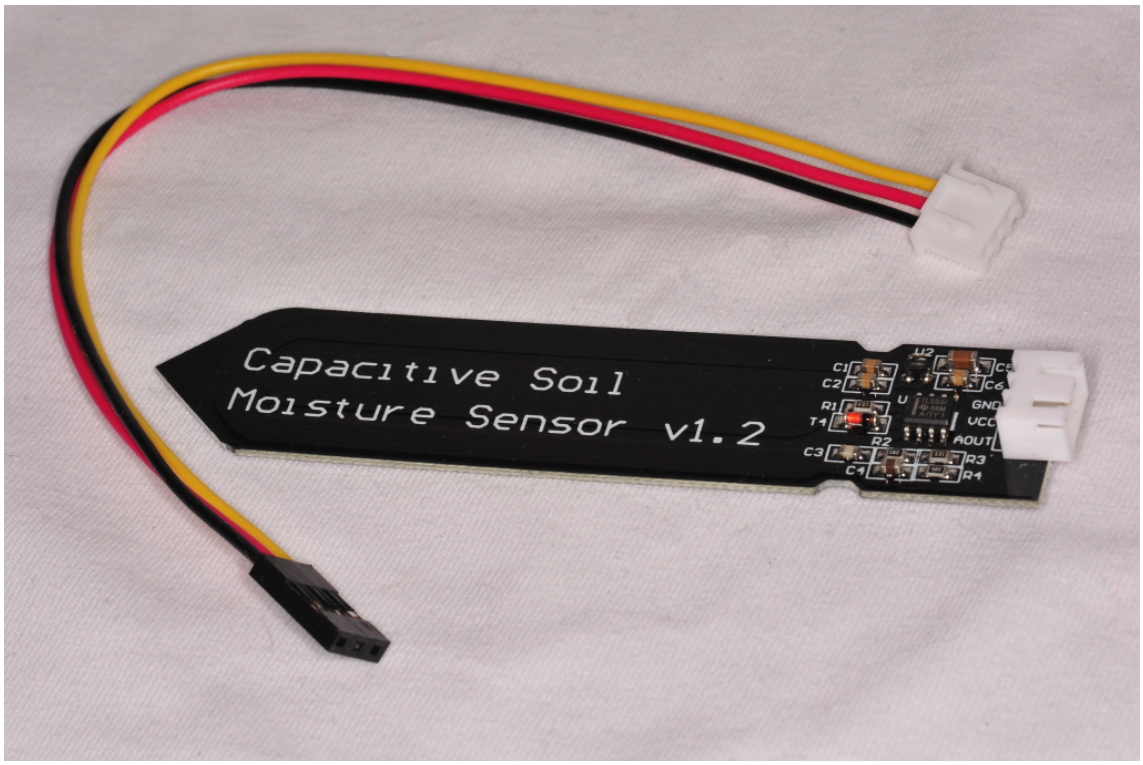

Fig. 3.7: Photo of the "Capacitive soil moisture sensor v1.2", purchased for evaluation (author)

3.4 Microcontroller

There is a lot of competition from microcontroller manufacturers in the market and therefore there's a wide variety of parts to choose from. The microcontroller unit (MCU) had to be chosen with regard to power consumption and sufficient computing power, yet still with suitable peripherals capable to operate sensors.

Because there were development tools by STMicroelectronics (STM) already available at the time of working on this thesis, the MCU by this manufacturer was chosen from their portfolio. STM offers STM32L0 series of 32-bit ultra-low-power MCUs based on ARM Cortex M0+ core in standard packages. From the "Value Line" of this series, the STM32L010RB in LQFP64 package was selected with regard to prototyping and hardware design, because it offeres the best capabilites of this line – the most peripherals and the most memory available from the L0x0 prudct line, as seen on figure 4.7. [5]

There are also various development boards available by STMicroelectronics, whicih enable quicker and more flexible prototyping. Therefore NUCLEO-L010RB equipped by the same MCU as selected above was put into testing along with developing the protype concept.[23]

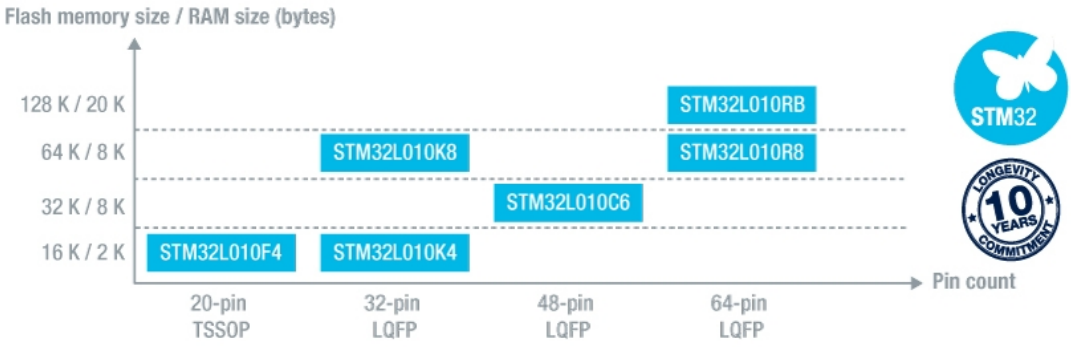

Fig. 3.8: STM32L0x0 Value Line [5]

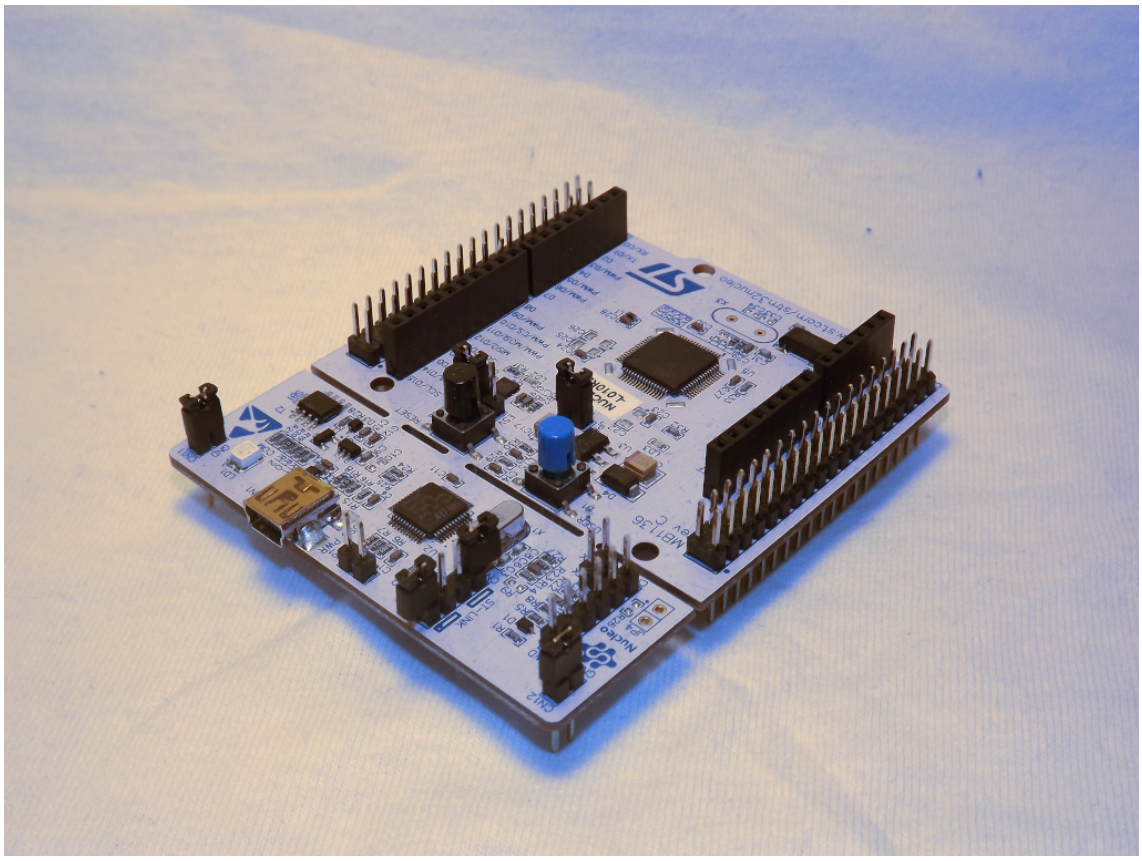

Fig. 3.9: STM32L0 Nucleo, purchased for evaluation (author)

3.5 LoRaWAN Connectivity

There are more approaches to implement hardware for utilizing LoRa modulation and eventually LoRaWAN protocol stack. Apart from designing the hardware and software completely from scratch, which would require a special use case and is in general not profitable for common use, there are off-the-shelf solutions available.

It is possible to either utilize a fully integrated module, which contains a microcontroller equipped with LoRaWAN protocol in its firmwarere and the radio part in one package, or a combination of stand-alone radio module connected to the host microcontroller with the protocol implemented on it separetely. Further described examples were primarily intended to be operated in 868 MHz band.

3.5.1 Standalone radio chips and radio modules

The SX1276 by Semtech is integreted circuit, which incorporates radio wireless LoRa moodulation transceiver interfaced via SPI. It is available on read-made printed circiut board module.

3.5.2 Integrated modules

There is a vast variety of integrated modules, which are usually operated by a standard communication interfaces like UART, SPI, I2C, etc. For purpose of testing, two were chosen – Microchip RN2483 and E-Byte E32-868T20D

RN2483

Microchip manufatired module with RF circuitry, LoRaWAN MAC accessibility. It operates in 868 MHz band with transmit power up to +14 dBm and is interfaced by UART. [24] Further description is in the next chapter.

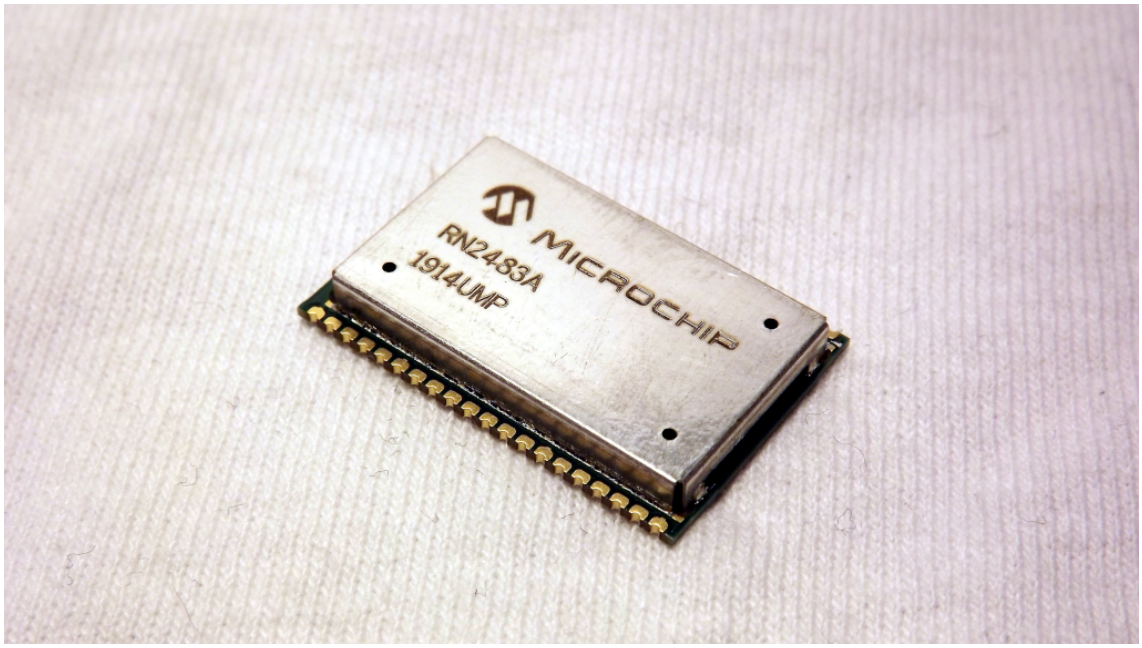

Fig. 3.10: Photo of RN2483 module, purchased for evaluation (author)

E32-868T20D

The E32-868T20D by E-Byte is an iteresting alternative to integrated modules. It provideas also UART interface and simillar parameters to RN2483.[25]

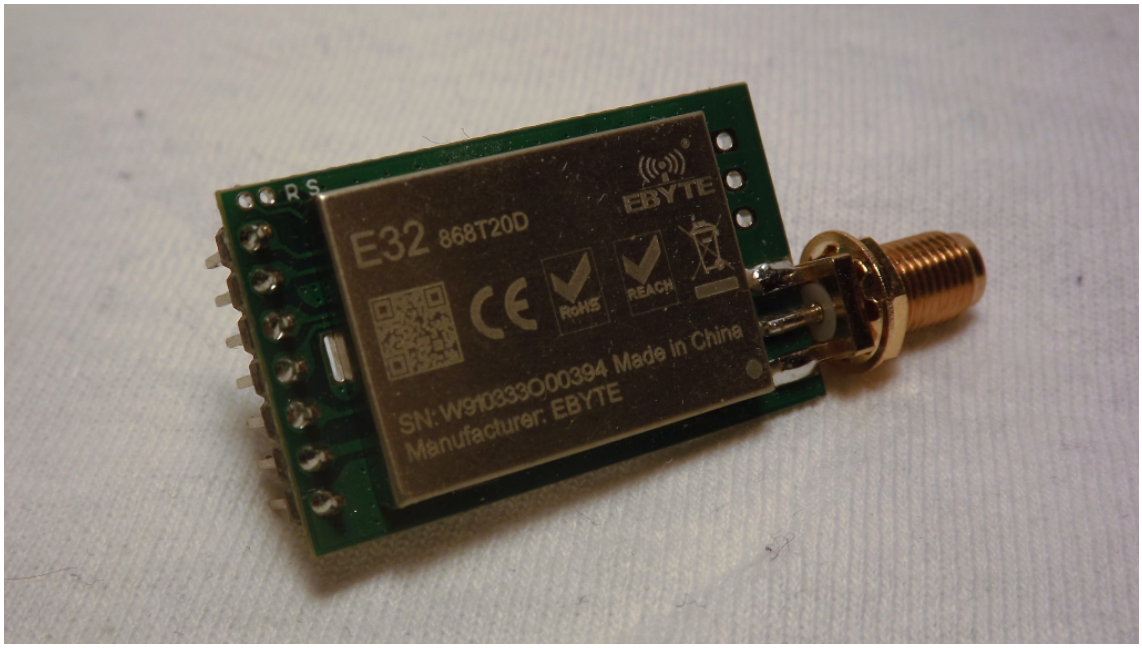

Fig. 3.11: Photo of Ebyte E32-868T20D, purchased for evaluation (author)

3.5.3 System on a Chip

Fig. 3.12: STM32WL annoucement; adopted from [6]

"System on a Chip" is an integrated circuit, which integrates a microcontroller (or a microprocessor) with advanced peripherals in one package. During working on this thesis, new possibilities immersed to the market in the field of LoRa integrated solutions – the STM32WL System-On-Chip was announced during the February

2020.[6] This is a system on a chip solution, which integrates both a general purpose microcontroller and a sub-GHz radio on the same chip.[6, 26] The design of the implementation in this thesis was nearly completed, therefore this option was not the subject of testing, yet it could be a useful core for future projects oriented on LoRa.

3.6 LoRaWAN Gateway

Gateways available on the market occupy a wide range of choices from designing one from scratch to off-the-shelf solutions. But there is usually a time and cost trade-off, which means when aiming for good time and price ratio, pre-built solutions can be the answer. Although there are cheap models, they are usually single-channel, which is not suitable for a larger network. Using Raspberry Pi one-board microcomputer together with iC880A concentrator board, an affordable, yet fully operable gateway can be built.[27] This way was chosen and is described in deatil in the next chapters.

4 The Prototype

This part of the thesis transforms theoretical assumptions and selected components into practical design of the measuring system. This part of the work describes applied approaches to integrate selected hardware into the system. The first protype of the measuring device is based on the conclusions made in previous chapters and aims to incorporate means of interchageability of parts used and therefore broader testing abilities to compare available solutions or to broaden capabilites of the system in the future.

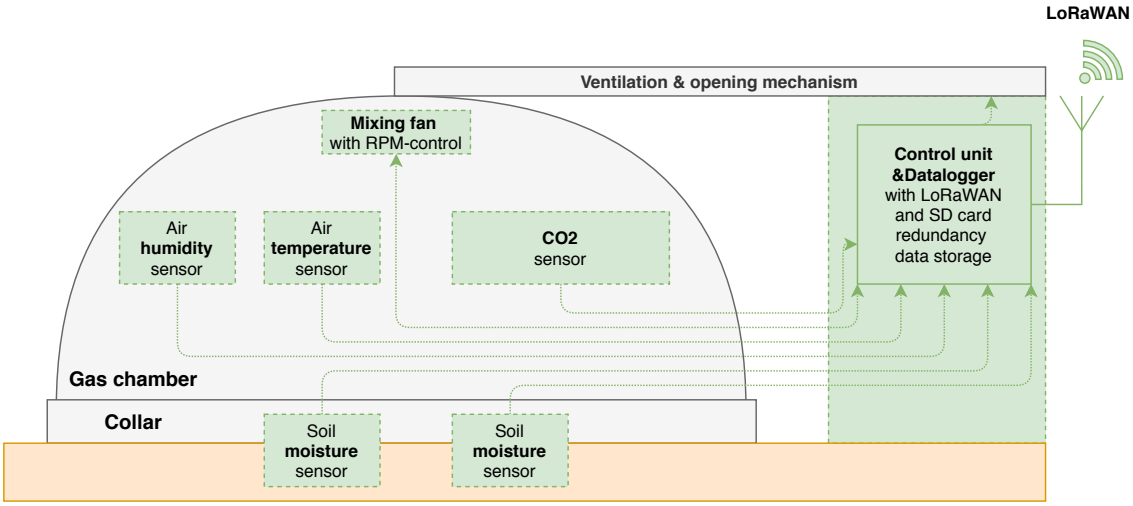

Fig. 4.1: Block diagram of designed apapratus (author)

All the hardware was designed using cross platform open Source software KiCad EDA (Electronic design automation, also referred to as ECAD, electronic computer-aided design).[28, 29]

4.1 Control Unit – "Control box"

Each sensor and actuator is operated by the control unit, named "Control box" in terms of this work, as well as in the schematic and PCB design attachments. The figure 4.2 shows functional sections of the Control box.

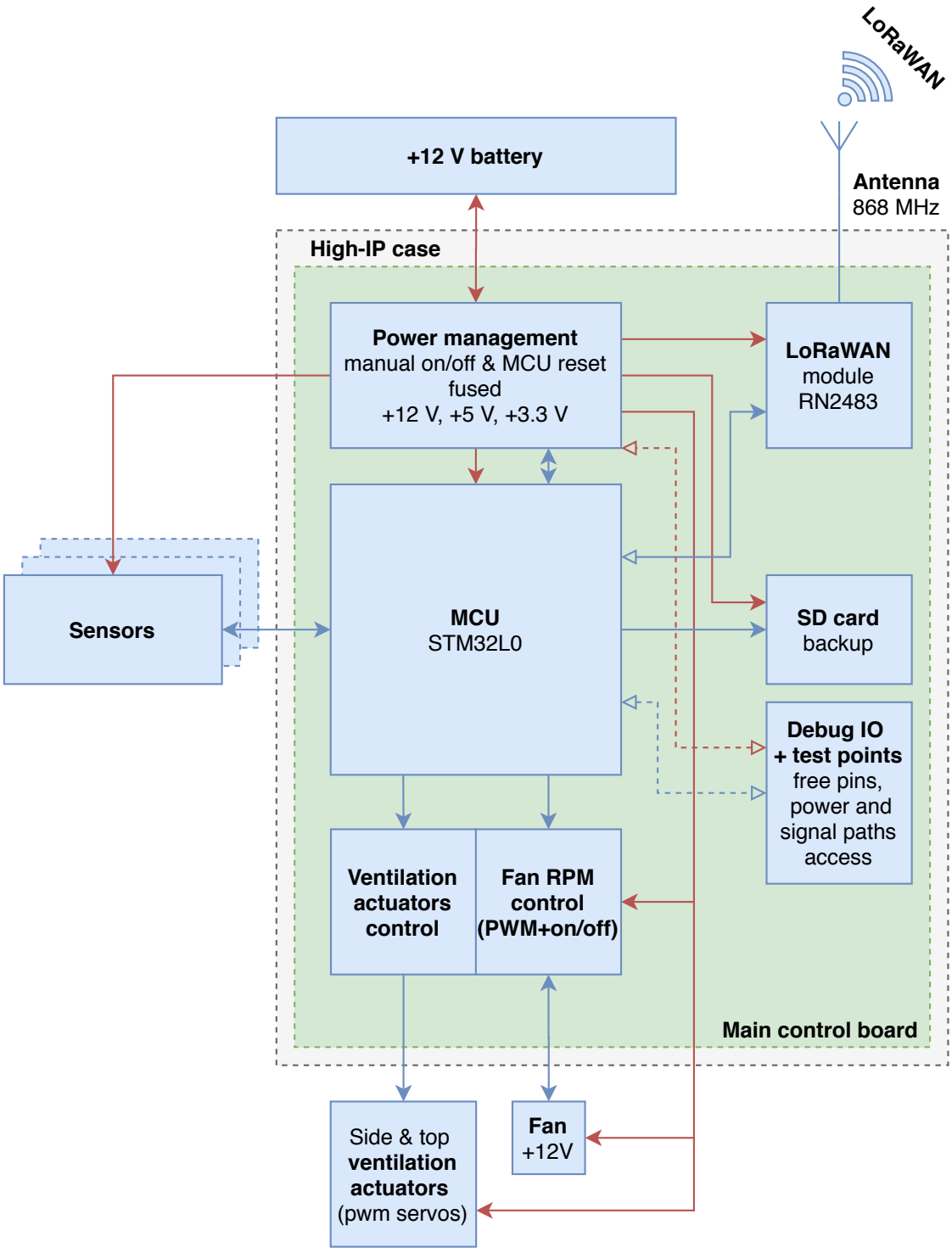

Fig. 4.2: Block diagram of control unit "Control box" (author)

4.1.1 Power Management

The device uses three DC voltage levels. The +12 V branch is delivered directly from the battery nominal voltage, which is intended to be twelve-volt maintenance-free lead battery or any simmilar kind of power source. The +12 V branch is used to power the mixing fan and two switching regulators, which are configured to provide +3.3 V and +5 V outputs both capable of delivering 2.5 A. The 3.3 V branch is used mainly to power the MCU, which then decides when to use the others depending on needed load usage (for exmaple sensors or the fan).

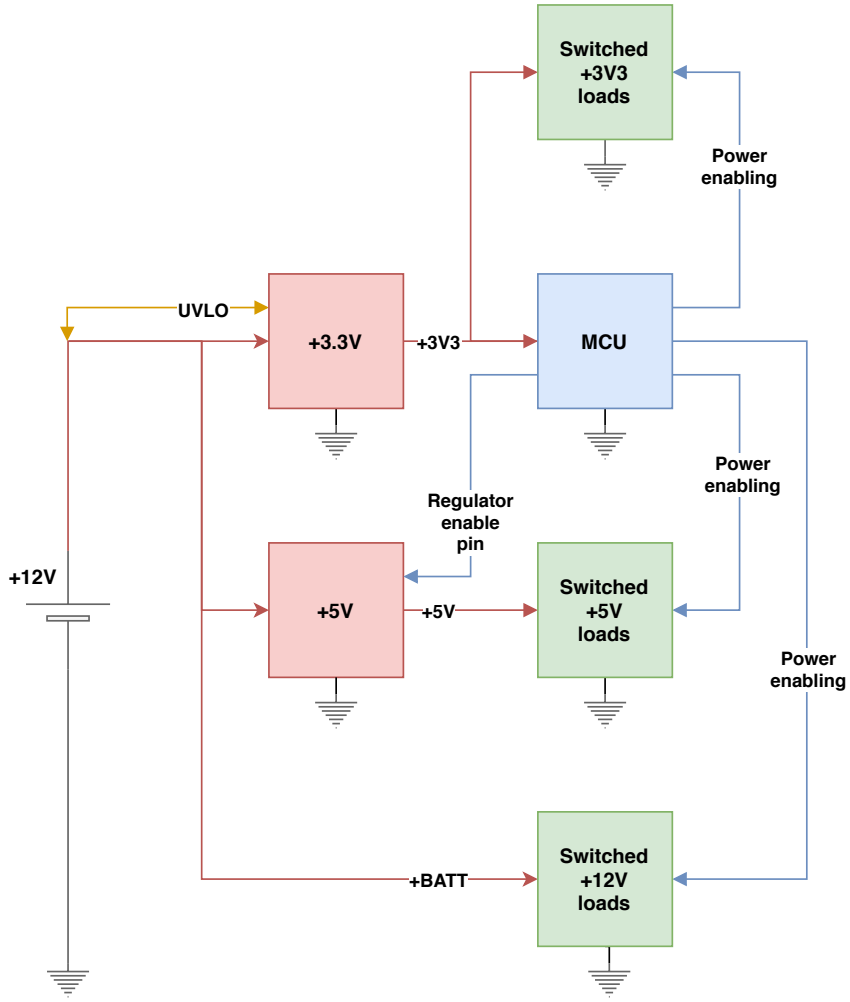

Fig. 4.3: Overall view on power levels and individual branches (author)

Switching regulators LM63625 by Texas Instruments were selected to control the power supply. The LM63625 is a very versatile switching regulator, which offers many variants of configuration options. The output volage can be set to fixed 3.3V, fixed 5V or adjusted to any voltage in range of 1 to 20 V, with respect to the input voltage able to go up to 40 V. [30, 7]

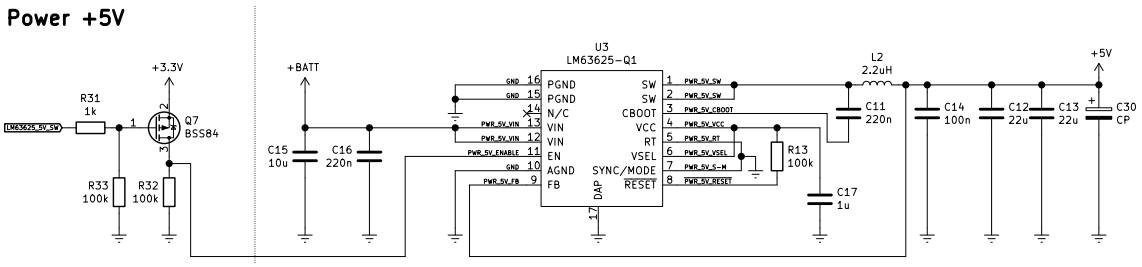

Fig. 4.4: The LM63625 set for +5V output, enabled programatically (author)

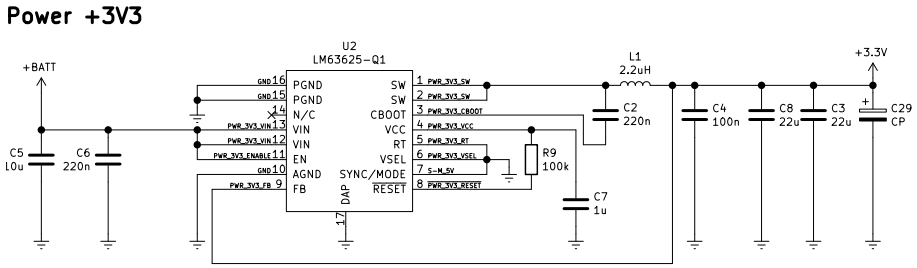

Fig. 4.5: The LM63625 set for +3.3V output, fixed enabling (author)

In order to keep the possibility of comparing the design with some verified results, the reference design of the switched converter according to the Texas Instruments documentation was finally used for both +5 V (figure 4.4) and +3.3 V (figure 4.5) voltage levels. The +5V branch is enabled programatically, while the +3.3V branch has fixed enabling for always enabled in the second prototype design iteration.

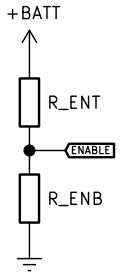

Fig. 4.6: The UVLO divider, from [7]

The third version shall have undervoltage lockout (UVLO) ability not to drain the battery under its limits. The UVLO is set by a voltage divider 4.6 from input voltage V_{IN} (V_{BATT}) for V_{OFF} turnoff voltage and V_{ON} turnon voltage respectively by simple equations 4.1 and 4.2 below.[7]

$$R_{ENT} = R_{ENB} \cdot (\frac{V_{ON}}{V_{EN-H}} - 1) \tag{4.1}$$

$$V_{OFF} = V_{EN-H} \cdot (\frac{V_{ON}}{V_{EN-H}}) \tag{4.2}$$

The parts selected to work with the switching regulator are chosen as per reference design. The first version of the hardware prototype power management was designed according to datasheet guidelines to reduce switching frequency from default 2.1 MHz to lower 400 kHz (adjustable downto 250 kHz), and therefore increase the efficiency, although with trade-off for bigger capacitors and inductors used. These efforts were thwarted by the imperfections in the soldering of the designed printed circuit boards in conditions of limited tool availability. With the former aim to achieve $f_{sw} = 400$ kHz selection of parts was done by following calculations. The inductor slection is described in [7] by following equation:

$$L = \frac{V_{IN} - V_{OUT}}{f_{sw} \cdot K \cdot I_{OUTmax}} \cdot \frac{V_{OUT}}{V_{IN}}, \tag{4.3}$$

where:

- V_{IN} – input voltage,
- V_{OUT} – output voltage,
- f_{sw} – switching frequency,
- K – ratio of ripple current over maximum output current, to be selected usually as 20–40% (K=0.2 to K=0.4),
- I_{OUTmax} – maximum output current.

Calculations were done for both corner-cases of both voltage levels managed by the regulators.

Assuming following values:

$I_{OUTmax} = 2.5$ A, $V_{INnominal} = 12$ V, $V_{OUTnominal} = 3.3$ V, $f_{sw} = 400$ kHz.

For $K = 0.2$ the $L = 11.9626 \cdot 10^{-6} H \approx 12\mu H$.
For $K = 0.4$ the $L = 5.9813 \cdot 10^{-6} H \approx 6\mu H$.
This would result in selecting 10 μH inductor.

Similarly for a voltage level of 5 V:

$I_{OUTmax} = 2.5$ A, $V_{INnominal} = 12$ V, $V_{OUTnominal} = 5$ V, $f_{sw} = 400$ kHz.

For $K = 0.2$ the $L = 14.5833 \cdot 10^{-6} H \approx 15\mu H$.
For $K = 0.4$ the $L = 7.2916 \cdot 10^{-6} H \approx 8\mu H$.
This would result in selecting 10 μH inductor.

There is also an equation to select output capacitors as well as for coping with their ESR (equivalent serial resistance):

$$C_{OUT} \geq \frac{\Delta I_{OUT}}{f_{sw} \cdot \Delta V_{OUT} \cdot K} \cdot \left[(1-D) \cdot (1+K) + \frac{K^2}{12} \cdot (2-D) \right], \tag{4.4}$$

$$ESR \leq \frac{(2+K) \cdot \Delta V_{OUT}}{2 \cdot \Delta I_{OUT} \left[1 + K + \frac{K^2}{12} \left(1 + \frac{1}{(1-D)} \right) \right]}, \tag{4.5}$$

$$D = \frac{V_{OUT}}{V_{IN}}, \tag{4.6}$$

where:

- ΔV_{OUT} – output voltage transient,
- ΔI_{OUT} – output current transient,
- K – ripple factor given in inductor selection.

Results of calculations are summarized in table 4.1 below.

Tab. 4.1: Output capacitor selection

Output voltage	**D**	**K**	**0.2**	**0.3**	**0.4**
3.3 [V]	**0.275**	**C [F]**	0.000108125	0.000132699	0.000182447
3.3 [V]	**0.275**	**ESR [Ω]**	0.054638881	0.052358212	0.050289017
5 [V]	**0.4167**	**C [F]**	0.000146925	0.000106967	0.000087264
3.3 [V]	**0.4167**	**ESR [Ω]**	0.054588406	0.052258559	0.050132580

4.1.2 MCU

The STM32L010RB in LQPF64 package was prepared according to STM application note on hardware development [31], which states the needed components and their use for the MCU to work properly.

Blocking capacitor values are reccomended 100 nF at each powering pin and one 10 μF for the whole package. The crystal oscilator recommendations propose formula 4.7 to pick rightmost value for the crystal load capacitors.

$$C_L = \frac{C_{L1} C_{L2}}{C_{L1} + C_{L2}} + C_{stray} \tag{4.7}$$

The C_{Ln} are tle load capacitors and C_{stray} is the pin capacitance and board or trace PCB-related capacitance typically between 2 pF and 7 pF. Value of 10pF was selected as a trade-off between theoretical calculation and rules of thumb, as

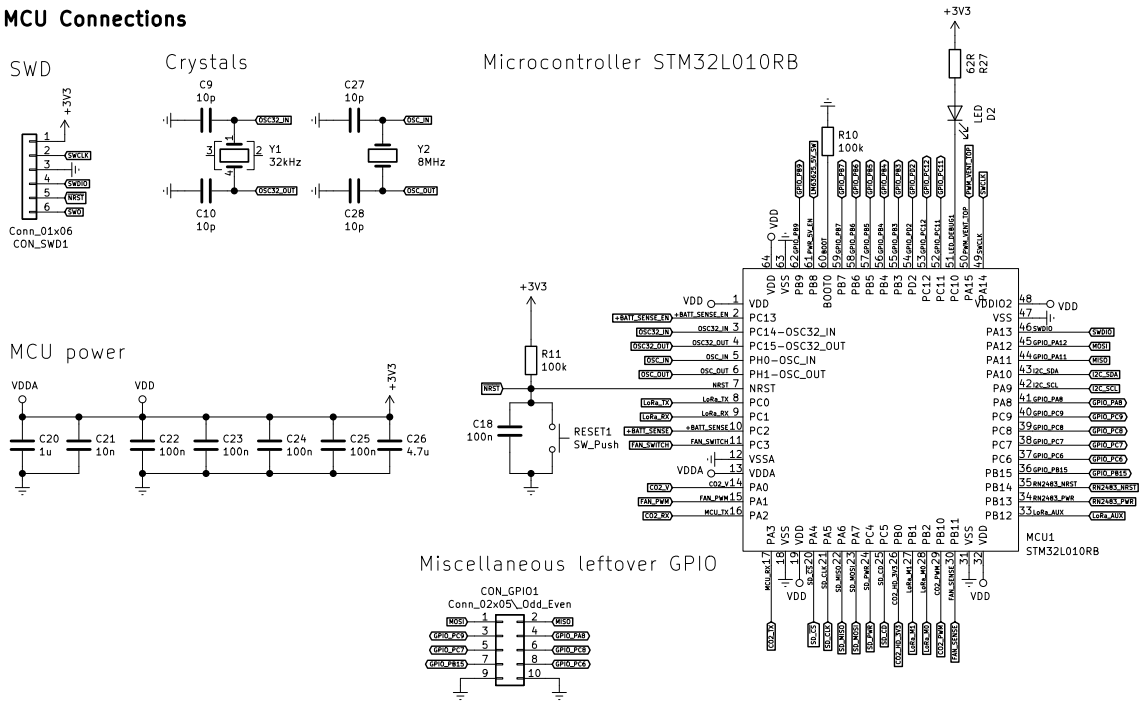

Fig. 4.7: MCU with its connections (author)

the manufaturer of 32 kHz CN250C crystal Citizen states 12.5 pF. [32] The high-speed crystal is experimental, not intended for primary use, as no high data rates are expected to be driven.

The programming interface and reset are wired as Single Wire Debug (SWD interface. This allows using directly STM Nucleo's built-in ST-Link as a programmer.[23]

All the used peripherals are described below. The LED on PC10 pin is there purely for testing purposes and can be programatically turned on and off. Besides all the used peripherals also several unused MCU pins were prepared on a breakout connector for debuging purposes or any potential expansion. Their selection was conditioned mainly by PCB space constraints.

Low-power modes

The selected MCU is equipped with modes to optimize power consumption, defined in 3 ranges by STM by frequency – range 1 up to 32 MHz, range 2 upt to 16 MHz and 3rd range limited up to 4.2 MHz. As there is no need to manage large data flows, the frequencies can be lowered dramatically and move the device to range 3 by default. On top of that, 7 low-power modes are available to find a trade-off between power consumption, startup time and wakeup sources from the sleep.

4.1.3 Communication

The RN2483 is used as primary connectivity module. It is manufactured by Microchip. The module is equipped by communication capabilities to use directly the LoRaWAN protocol a device in class A.

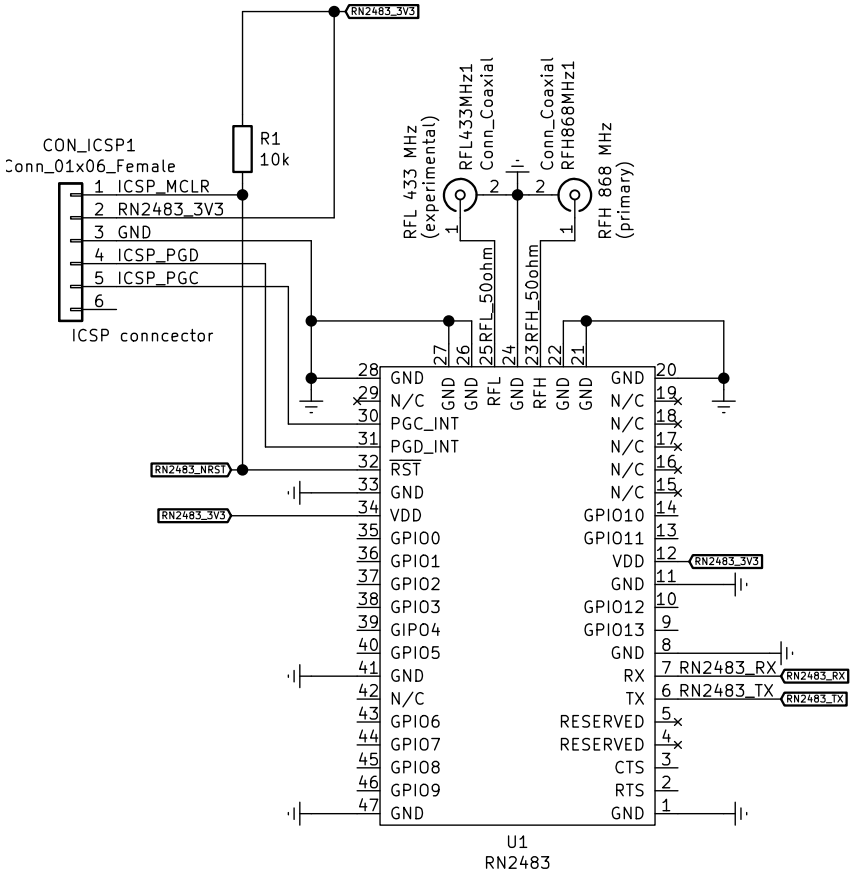

Fig. 4.8: Wiring diagram of communication module RN2483 (author)

Powering is rated for 3.3 V with maximum current draw of 38.9 mA when transmitting with maximal power 14 dBm. With this in mind, also the powering BSS84 P-MOSFET was selected with capability to handle 130 mA continuous drain current.[33] The module can operate in 868 MHz as well as 433 MHz band. As seen on 4.8, both antennas can be connected (and have corresponding footprints prepared on the PCB; see attachments), but primary use is intended in 868 MHz marked RFH, the second – RFL – antenna is not intended for normal operation in this design, only for any future experiemtnal use. Both antennas shall have matched impedance of 50 Ohm. The datasheet contains requirements for the design of the high-frequency part of the printed circuit board in the area of antennas and their respective SMA connectors for which the module is certified. These requirements have been strictly adhered to in order to comply with this application note. The

ICSP connector serves for firmware updates of the module, having the reset pin also connected to the MCU to control it programatically.[24]

MCU also hnadles the UART interface. As the RN2483 offers auto-baud detection, the MCU can adapt it to STM's LPUART by changing the default set baudrate 57600 bps to 9600 bps, while keeping 8 bit length with no parity, 1 stop bit and no flow control. Commands are sent in ASCII character format. There are three basic types of command: "sys" for system commands, "mac" for working with LoRaWAN MAC layer, and "radio" serving for configuration and data acquisition from the radio part of the module.[34]

The RN2483 is intended to be used as primary module, therefore is prepared to be soldered on the PCB. On top of that, the design allows for the possibility of disconnecting the primary module via pinheaders and connecting, for example, the module from Ebyte instead, or any other that supports UART, as seen on 4.9. The other signals mentioned (M0, M1, AUX) are intended for the Ebyte E32-868T20D [25], but can be reconfigured to GPIO of choice depending on module used.

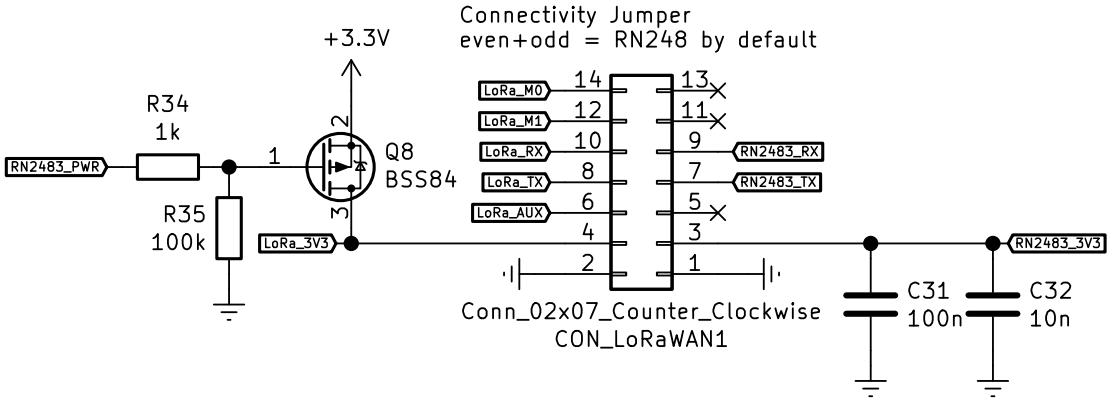

Fig. 4.9: Wiring diagram of communication module connector (author)

4.1.4 Homogenization fan

For the chamber ai homogenization a 4-pin PWM-controlled PC fan is used to minimize costs and simplify controlling of its speed. The figure 4.10 shows the sognals of the fan, whcih are connected to the MCU. The MCU controls the fan with FAN_PWM signal, translated by Q5 from 3.3V to 5V level. The FAN_SWITCH switches the fan via NPN and N-MOSFET transistor pair Q3 and Q5. The FAN_SENSE can be used for counting pulses send by the fan each two revolutions as a feedback.[35]

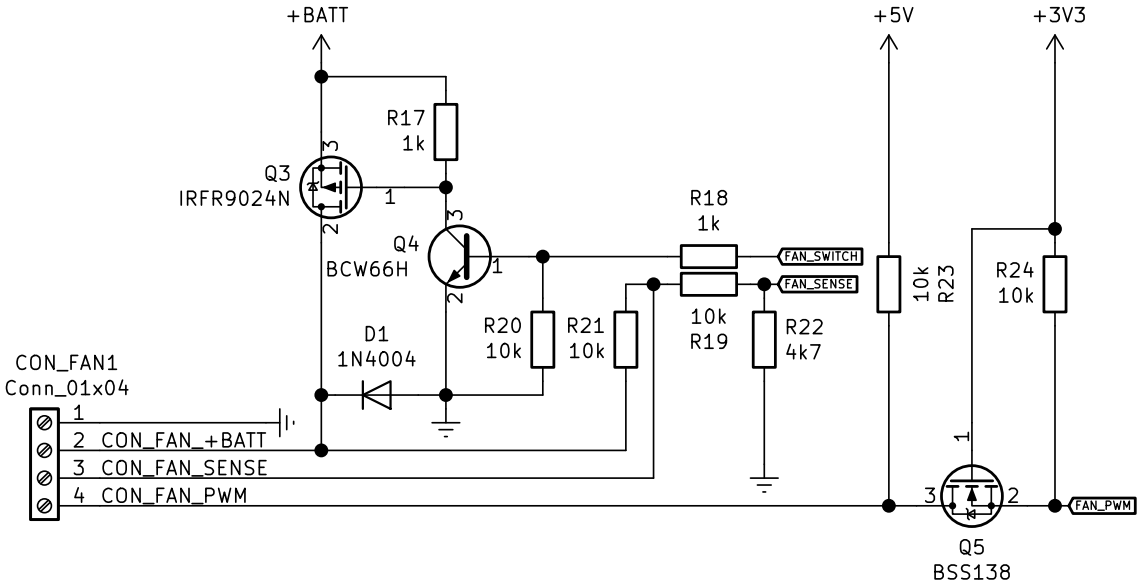

Fig. 4.10: Wiring diagram of the homogenization fan (author)

4.1.5 Redundancy storage – SD Card

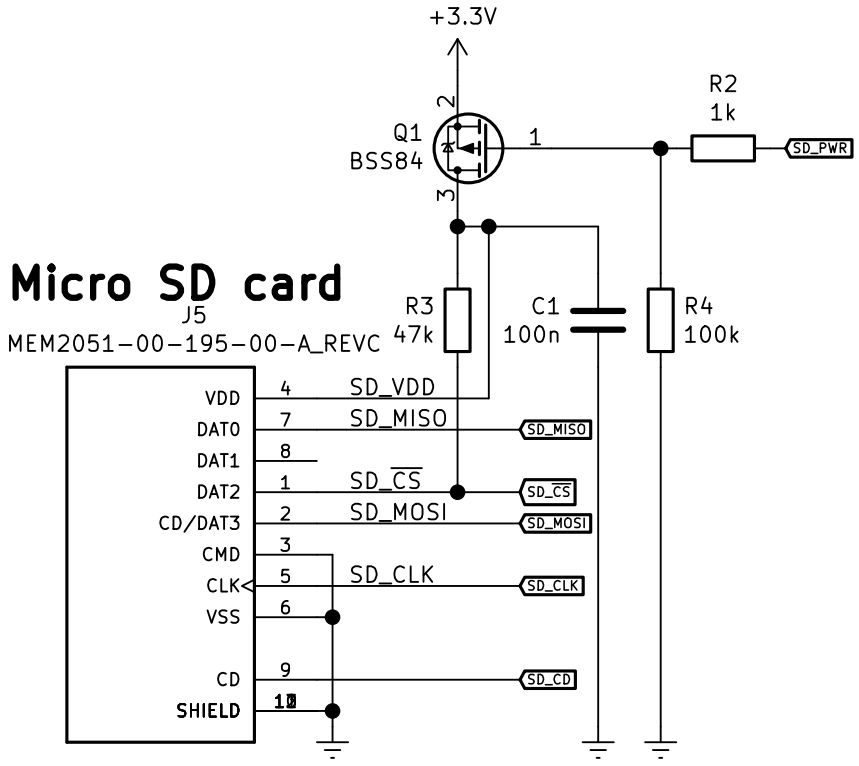

Fig. 4.11: Wiring diagram of the SD card redundancy storage (author)

The device has a possibility to utilize on-board SD card slot. It was prepared to broaden usability of the designed device in places, where signal coverage would be

bad or even impossible (underground), and for ability to achieve redundancy when needed. The figure 4.12 shows SD card part of the schematic. The card works in SPI bus mode and can be powered on and off to save power when unused by Q1.

4.1.6 Other peripherals

All the other sensors, actuators and peripherals can be connected to the main board with practical screw-on terminal blocks.

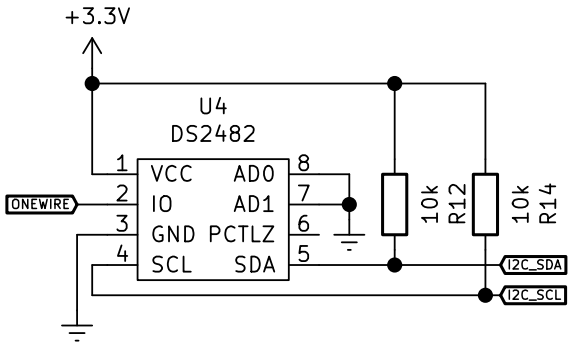

Fig. 4.12: The DS2482S-100 One-Wire to I2C translator (author)

Thermometers are using One-Wire bus, therefore to simplify accessibility to the bus by the MCU, integrated circuit DS2482S-100 was used to provide bidirectional protocol conversion between the I2C master and 1-Wire slave devices.

4.1.7 Firmware and logic

The device shall automatically start to independently control the entire measurement process immediately after switching on at the measuring site, unless otherwise stated. The flowchart 4.13 shows logical steps of the whole process. Brief explanatory of used abbrevations in 4.13:

- T_{vent} – period of ventilation (opened chamber),
- T_{warmup} – warmup time for sensors,
- $T_{mperiod}$ – period of between each data acquisition within one measurement cycle,
- $T_{wholement}$ – period of the whole measurement cycle.

The measurement shall take place once every given time $T_{wholement}$ and each measurement is split into several sample obtaining $T_{mperiod}$. After starting up the MCU is initialized, all the peripherals including the radio module and join attempt is preformed. Depending on the network response the data shall get stored in situ or send over the air. This is decided for the whole run time from this point on. Then after set period the chamber gets ventilated with fresh air, closed and the measurement starts. After the whole process the device performs a self-check. Battery is measured, set constrains are checked (i.e. desired number of measurements, forced data storage medium, etc.). If self-check passes, the device either continues or goes to hibernation. Sleep modes shall be entered during all waiting parts.

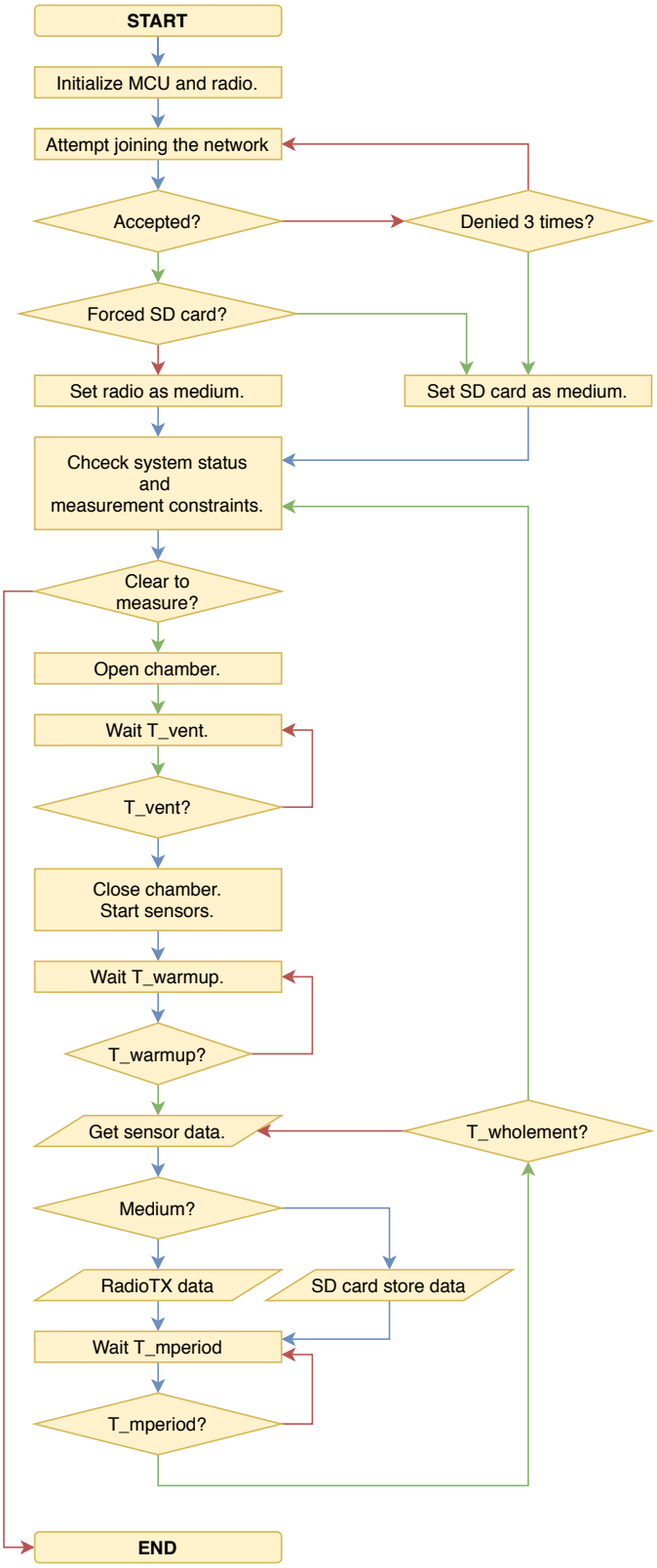

Fig. 4.13: Logic flowchart of "Control box" operation (author)

4.2 LoRaWAN Gateway – "Gateway box"

The LoRaWAN Gateway is based on The Things Network (TTN) services, which is an open infrastructure for the Internet of Things with community version usabe for free.[8]

Fig. 4.14: Logo of The Things Network, adopted from [8]

4.2.1 Hardware

On the TTN website there is a tutorial on utilizing a small single-board computer called Raspberry Pi together with IMST iC880A-SPI LoRa Concentrator board in order to build own user gateway for LoRaWAN. [27] This tutorial was used as an inspiration and a gateway was built with Raspberry Pi 3 Model B+ [36] and iC880A board [37].

A special connection board was designed modifying an open hardware project by openiot.network [38] for signal and mechanical connection of the used hardware. The table 4.2 shows the minimal required signals needed.

On top of that, a standalone integrated DC-DC switching power module Mean Well SCW12-A. The SCW12-A is capable of delivering +5 V and up to 2.4 A [39], which is sufficient enough for both the Raspberry Pi B+ (running headless), [40] and the concentrator [37]. The custom interface board also includes a jumper for connecting a mechanical power switch and basic input voltage polarity protection.

The gateway uses +3 dBi 868 MHz stick 90°/180° SMA omnidirectional antenna, which is connected by pigtailed coaxial cable to the iC880A board.[41]

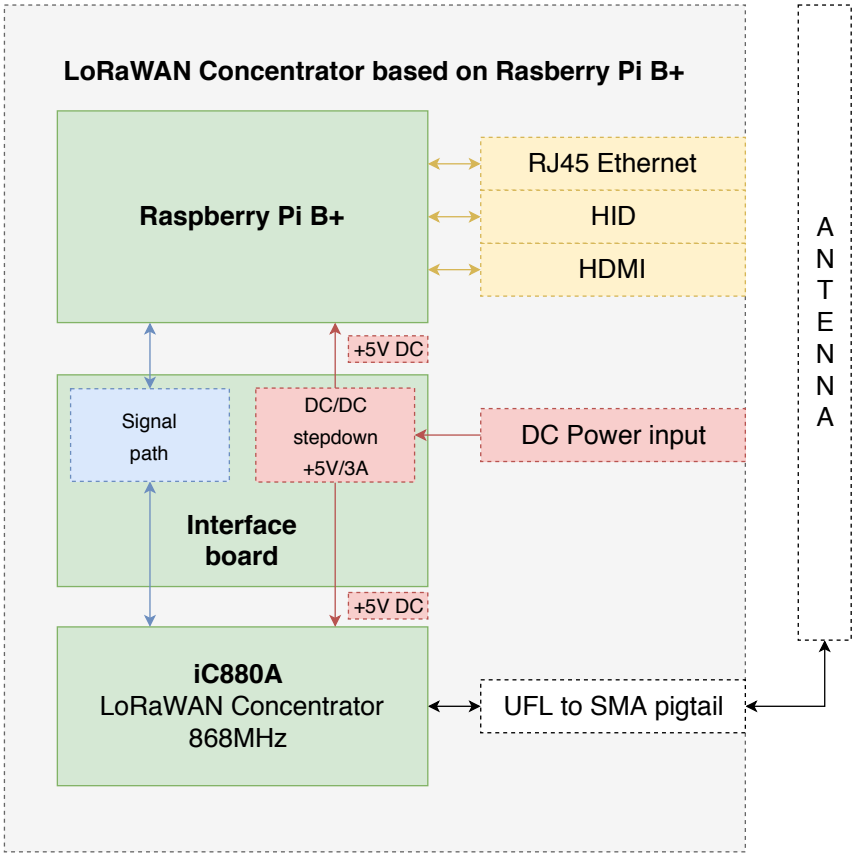

Fig. 4.15: Block scheme of the gateway (author)

Tab. 4.2: Minimal signal interconnection requirements between raspberry Pi and iC880a, adopted from [9]

iC880a pin	Description	Raspberry Pi pin
21	+5V	2
22	GND	6
13	Reset	22
14	SPI CLK	23
15	SPI MISO	21
16	SPI MOSI	19
17	SPI CS	24

The Raspberry Pi is running headless (without any desktop environment) Raspbian Lite [42], which was configured to support SPI-connected iC880A and works as a package forwarder to TTN services, as described in [9].

4.2.2 Infrastructure

After creating an account and siging in on the "TTN Console" the user can manage "Gateways" and "Applications" sections. In the Gateways section the gateways can be registered to TTN Console by its unique EUI identifier. Applications then offer registering individual devices for the network or specify their data payload format. An important part are the Integrations, which allow to pass the received data to other services, such as some cloud storage, other on-line services or – as in this case Google Sheets. It is available for free and offers an Excel-like tables to work with the data further. And as there was no need to present the data publicly, it sufices for this purpose more than enough. If any future use case would require a change, TTN allows to change the integration or add more for the same application.

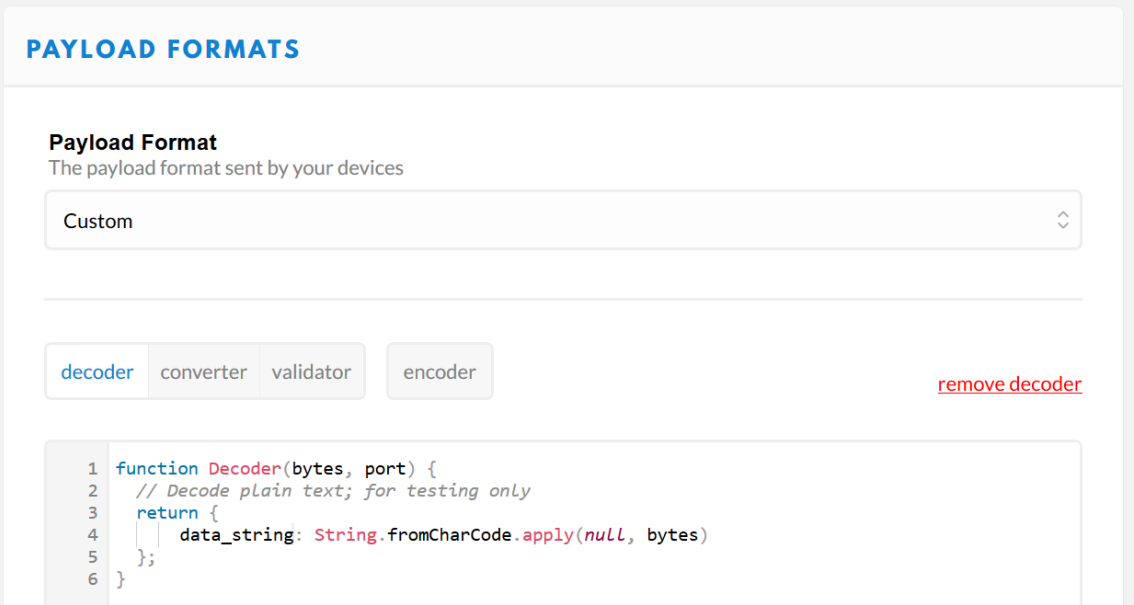

Fig. 4.16: Cropped screenshot of the TTN Console payload formater, showing simple string incomming to variable data_string (author)

Using Integration a HTTP INtegration was added, which sends uplink data to an endpoint with HTTP POST method and receives downlink data over HTTP. On the side of Google Sheets an empty sheet was created. When opened, in Tools there is option Script editor, which allows the user to configure behavior of the file. A script based on publicly accessible github projects [43] was created in this environment. It then needs to be published as web application and finally an URL is obtained, which is then inserted in the TTN HTTP Integration.

The TTN and Google Sheets allow to operate with json data format. The json shall be used with the data throughout the whole process from transmitting to storing the data, as it simplifies the data handling.

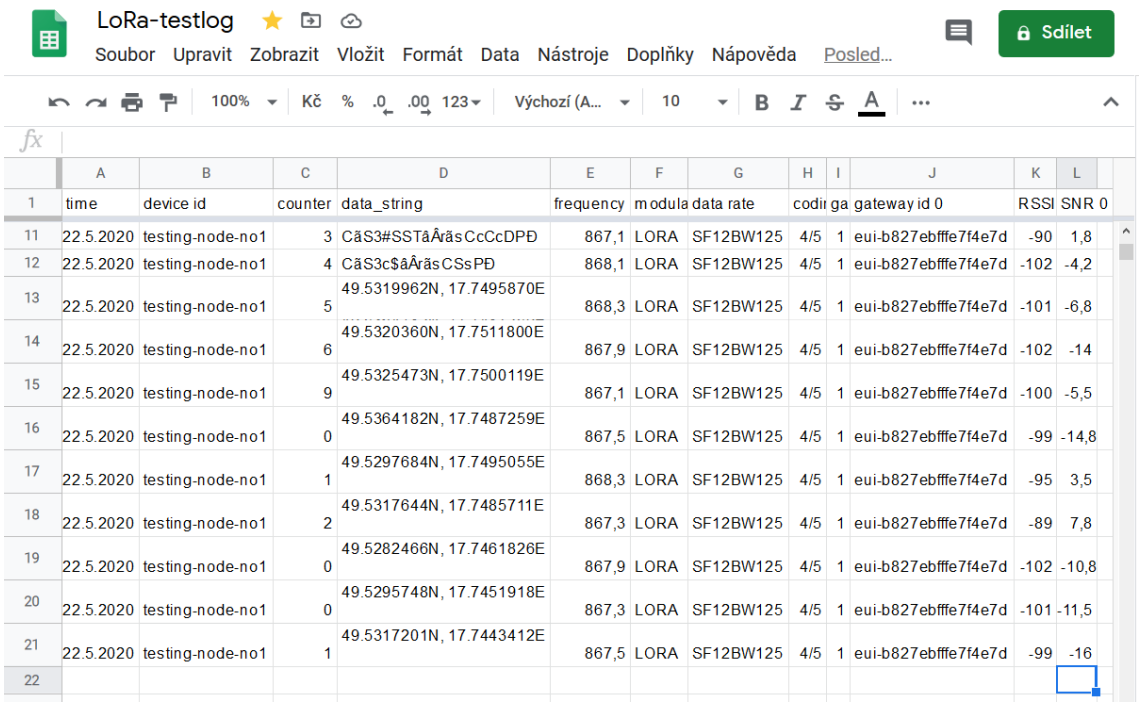

	A	B	C	D	E	F	G	H	I	J	K	L
1	time	device id	counter	data_string	frequency	modula	data rate	codi	ga	gateway id 0	RSSI	SNR 0
11	22.5.2020	testing-node-no1	3	CăS3#SSTâÅrăsCcCcDPĐ	867,1	LORA	SF12BW125	4/5	1	eui-b827ebfffe7f4e7d	-90	1,8
12	22.5.2020	testing-node-no1	4	CăS3c$âÅrăsCSsPĐ	868,1	LORA	SF12BW125	4/5	1	eui-b827ebfffe7f4e7d	-102	-4,2
13	22.5.2020	testing-node-no1	5	49.5319962N, 17.7495870E	868,3	LORA	SF12BW125	4/5	1	eui-b827ebfffe7f4e7d	-101	-6,8
14	22.5.2020	testing-node-no1	6	49.5320360N, 17.7511800E	867,9	LORA	SF12BW125	4/5	1	eui-b827ebfffe7f4e7d	-102	-14
15	22.5.2020	testing-node-no1	9	49.5325473N, 17.7500119E	867,1	LORA	SF12BW125	4/5	1	eui-b827ebfffe7f4e7d	-100	-5,5
16	22.5.2020	testing-node-no1	0	49.5364182N, 17.7487259E	867,5	LORA	SF12BW125	4/5	1	eui-b827ebfffe7f4e7d	-99	-14,8
17	22.5.2020	testing-node-no1	1	49.5297684N, 17.7495055E	868,3	LORA	SF12BW125	4/5	1	eui-b827ebfffe7f4e7d	-95	3,5
18	22.5.2020	testing-node-no1	2	49.5317644N, 17.7485711E	867,3	LORA	SF12BW125	4/5	1	eui-b827ebfffe7f4e7d	-89	7,8
19	22.5.2020	testing-node-no1	0	49.5282466N, 17.7461826E	867,9	LORA	SF12BW125	4/5	1	eui-b827ebfffe7f4e7d	-102	-10,8
20	22.5.2020	testing-node-no1	0	49.5295748N, 17.7451918E	867,3	LORA	SF12BW125	4/5	1	eui-b827ebfffe7f4e7d	-101	-11,5
21	22.5.2020	testing-node-no1	1	49.5317201N, 17.7443412E	867,5	LORA	SF12BW125	4/5	1	eui-b827ebfffe7f4e7d	-99	-16
22												

Fig. 4.17: Cropped screenshot of the Google Sheets with received data in column D – coordinates from experiments with RSSI measurements (author)

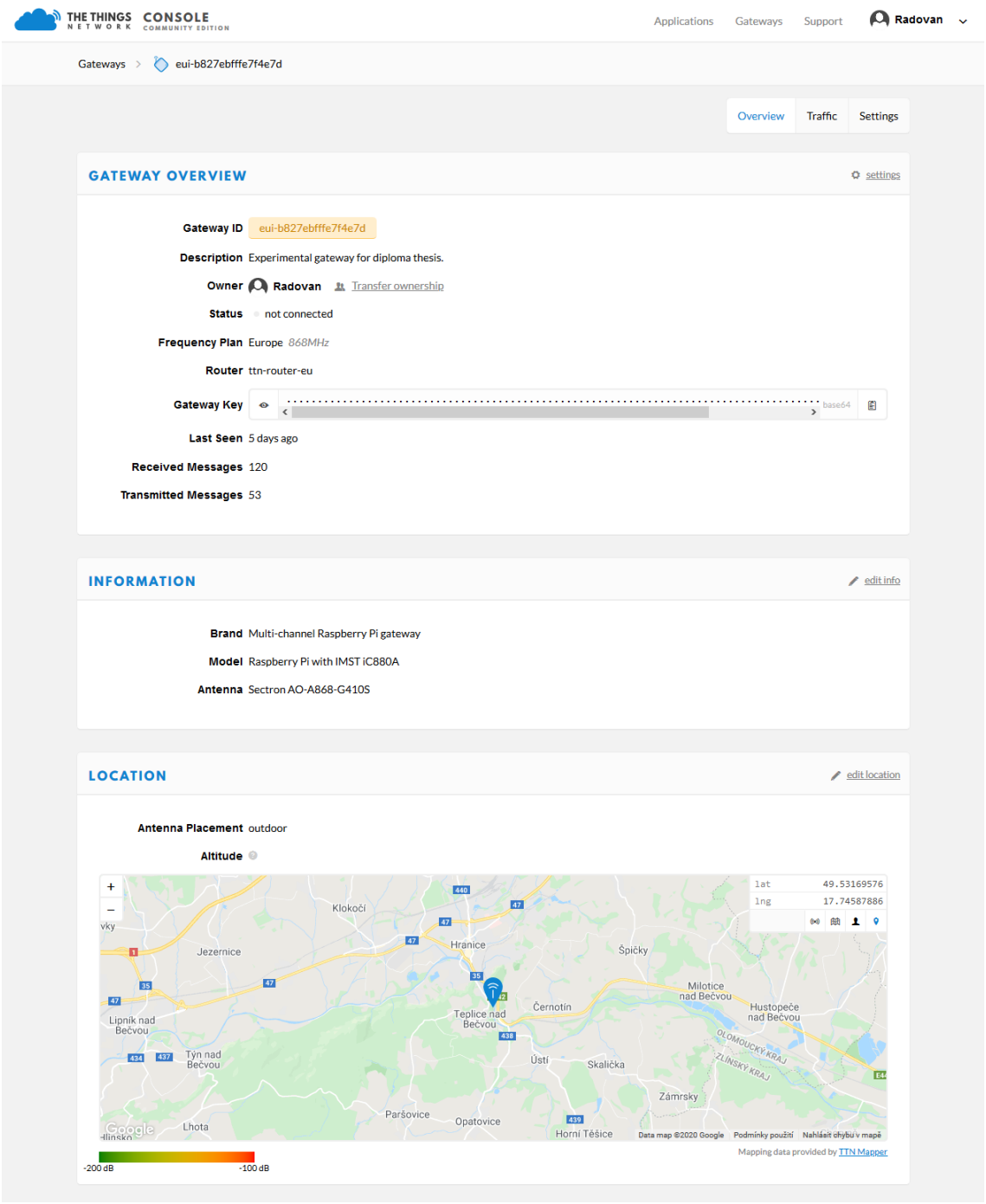

Fig. 4.18: Cropped screenshot of the TTN Console Gateway overview, gateway offline at the moment of taking the screenshot (author)

4.3 The Chamber

The prototype of the chamber was constructed from available and not costly materials, as seen on figure 4.22.

Fig. 4.19: Materials used for the chamber (author)

The main body is made of a sturdy wastepipe sleeve of 250 mm diamter covered with clear plexi glass. The sleeve contains two gaskets, one of which can be removed from the inside, inverted and then used as a gasket around the pipes outer diameter to create relatively tight seal between the plexi glass and the rest of the chamber. The second gasket can stay in palce and be used to fit on a collar made of wastepipe of this so called "KG" system, which fits in tight.

The opening is done with small, yet powerful +5 V DC PWM motor TowerPro 946R and a very simple arm made of two L-shaped pieces of metal screwed together, but left free enough so the arm cand bend and lift the lid with the third small piece of metal.

For easier cable management the Control box is equipped with a cable gland with JZ-500 multiwire cable interconnecting it via second gland with the inside of the chamber. In the place where the seal was located, a fold in the material of the sleeve remains after it. This fold is used to place a holder made of piece of metal in the chamber for the sensors and the homogenization fan.

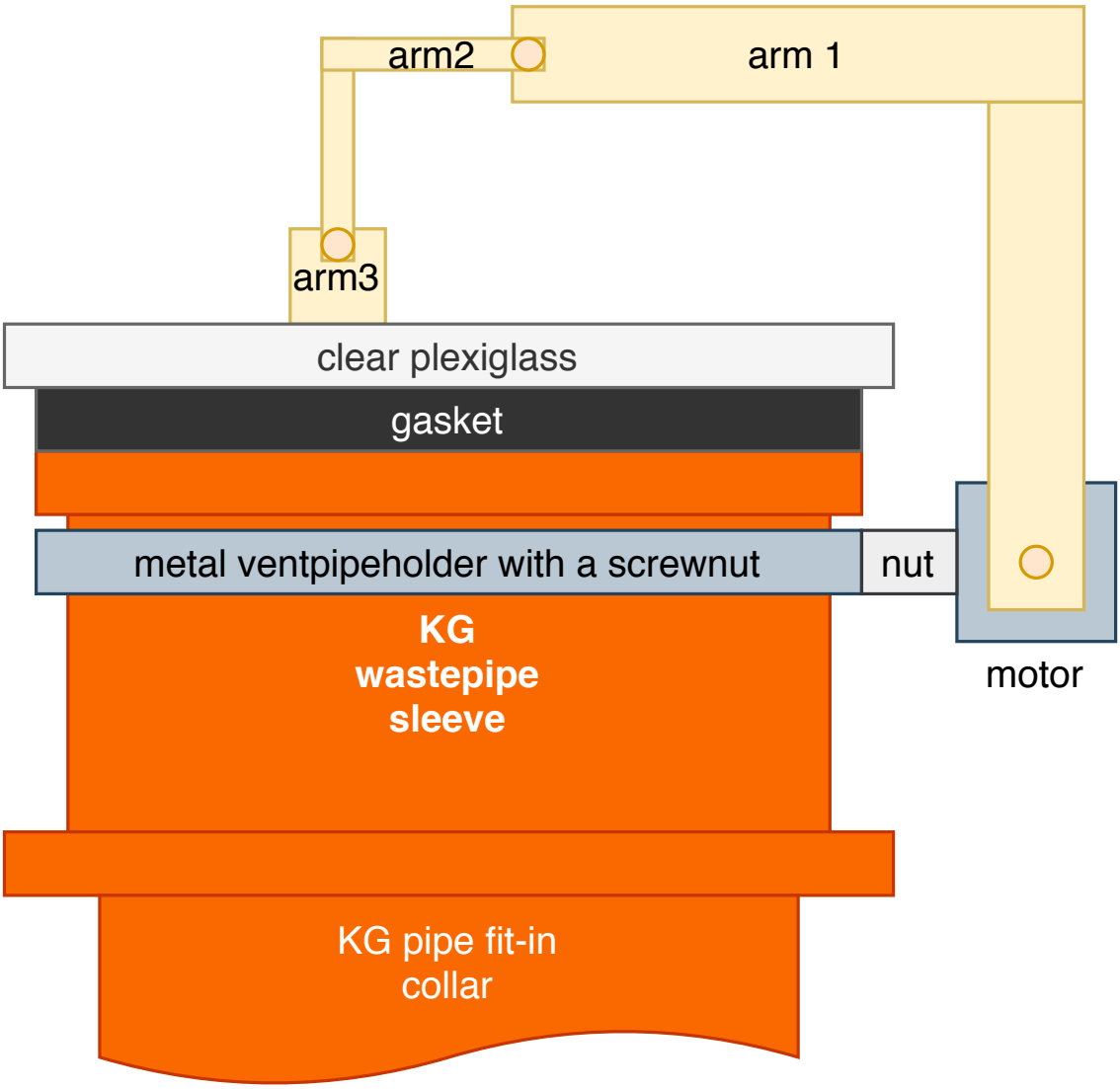

Fig. 4.20: The chamber system drawing, outside (author)

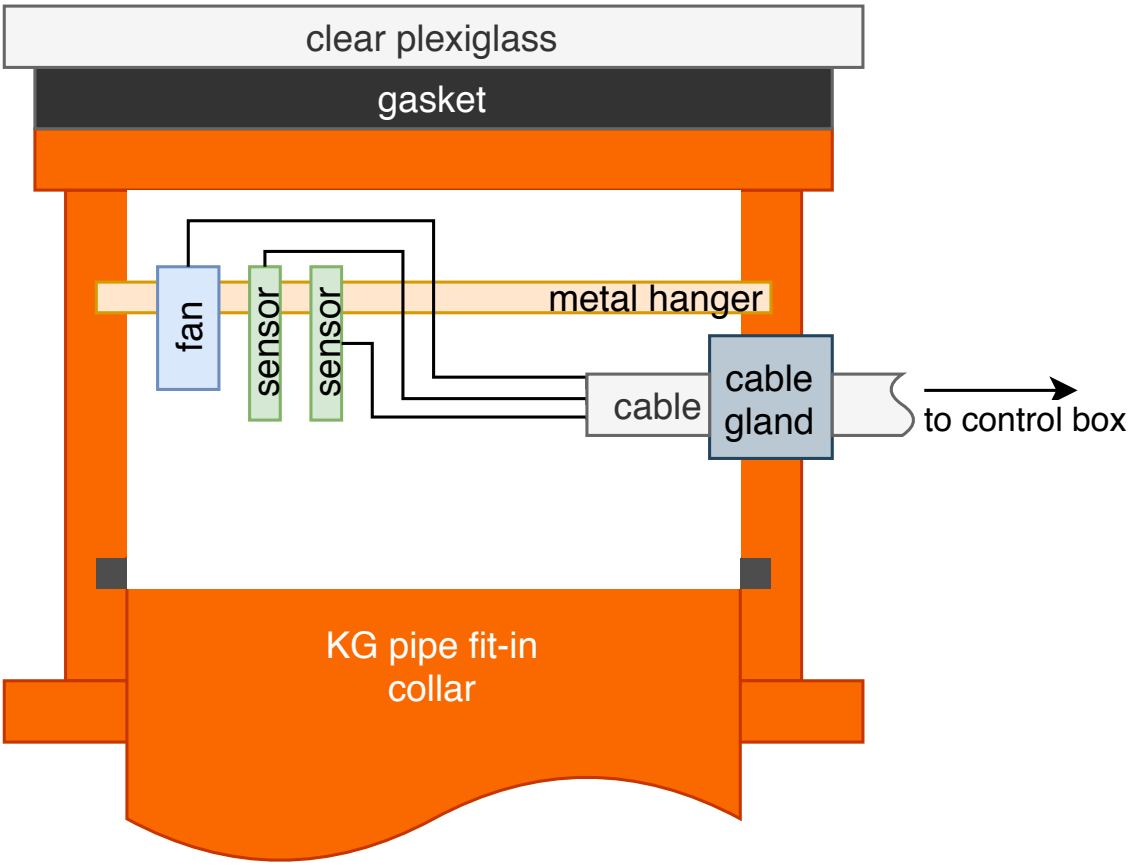

Fig. 4.21: The chamber system drawing, inside (author)

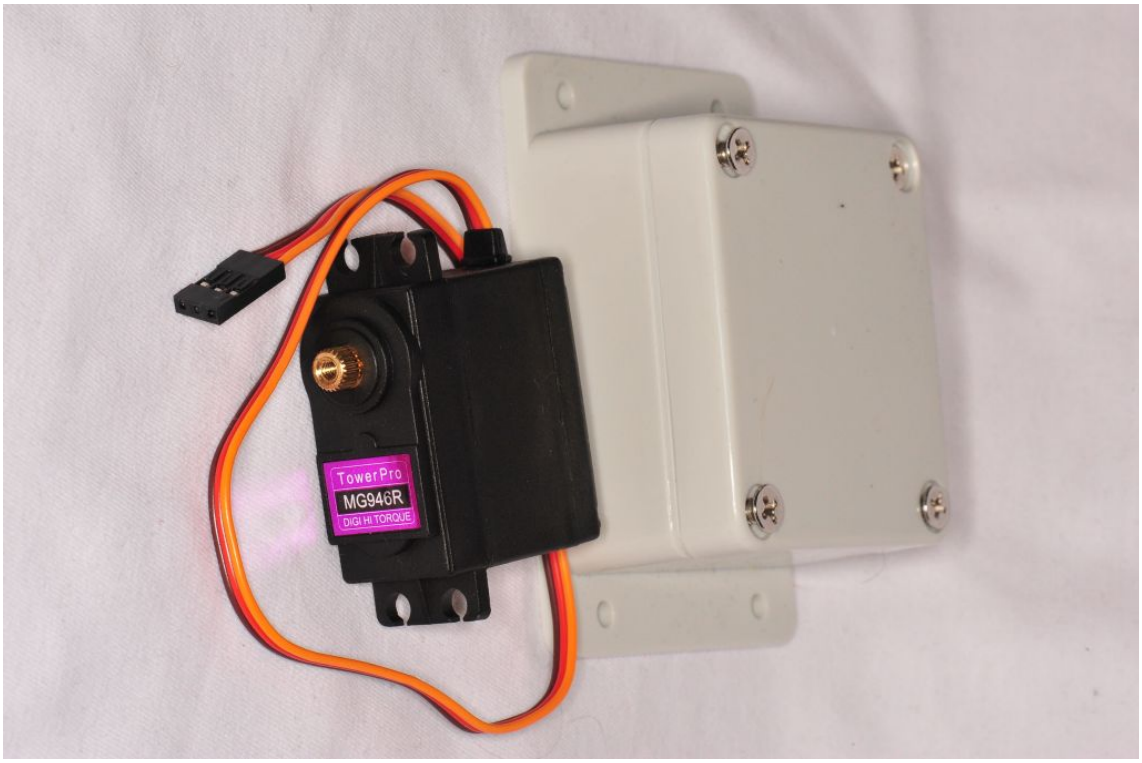

Fig. 4.22: PWM motor (author)

5 Results

Most of the results were presented continuously in the text of the thesis, however, this part is devoted to their summary and overall evaluation. It represents the achieved and fulfilled goals, but also the weaknesses of the work and their possible improvements.

5.1 The Control box

The device proposed in previous chapters was manufactured in 3 functional prototype exemplars. One of them can be seen on figure 5.1 with its blue testing (debug) LED turned on, after being programmed with Nucelo. Although the hardware works, the software is still only a working demo version, which is able to work with individual peripherals, but does not work yet as the system should as a whole. The system developmend carries on using STM tools CubeMX and CubeIDE.

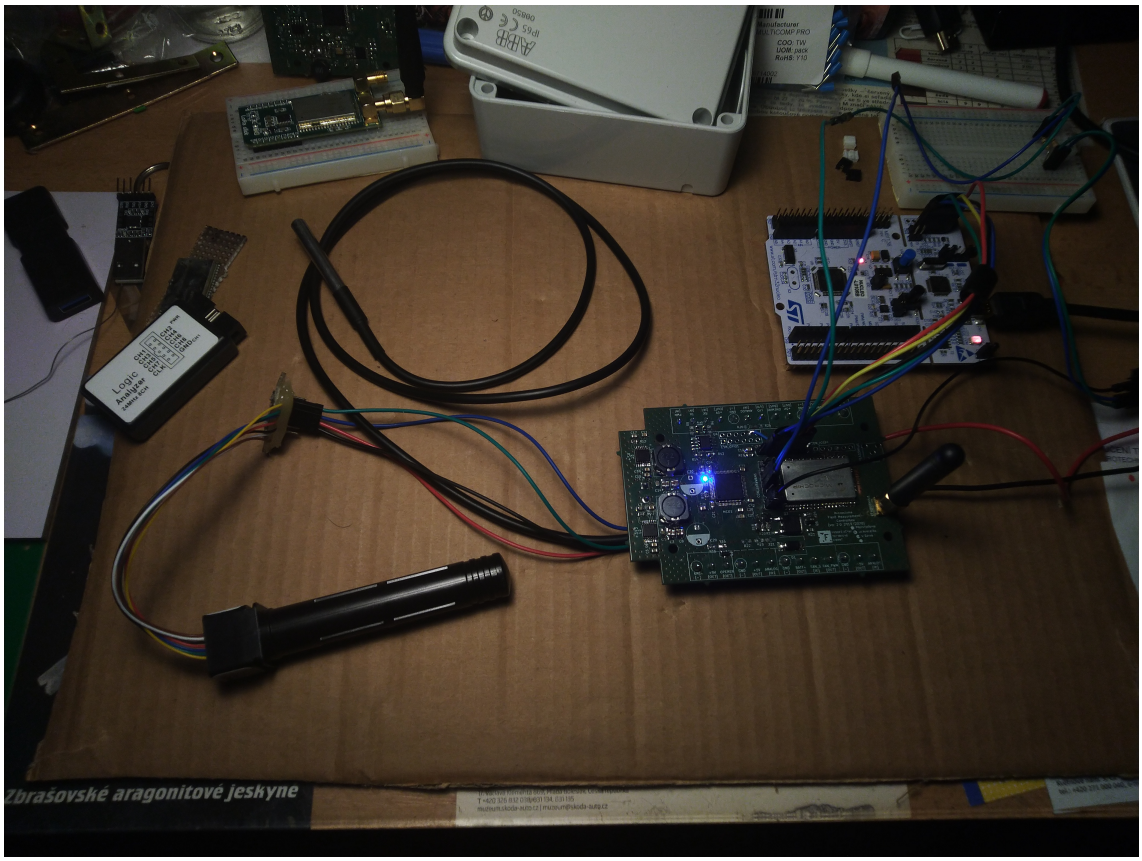

Fig. 5.1: Testing of the Control box (author)

5.2 The Gateway box

As presented in previous chapters, the gateway is fully operational and tested. When it comes to any improvements, a better and stationary position shall be find to improve signal reception, as during the experiments the gateway layed simply on the table in the upper floor of the ZAC administration builing, yet performed quite well.

5.3 The Chamber

Previous chapters shown the whole concept of a cheap, easy-to-build gas chamber. This concept was not validated and will get improved by empirical experiments and comparing to existent non-automated chambers and probably will adopt one of them intead and continue development on it.

5.4 LoRaWAN in open terrain of Bečva river valley

Based upon theory, LoRa modulation should be able to penetrate through harsh conditions of the communication channel over a large distance. In order to verify that the selected wireless network infrastructure, a simple measurement of the received signal strength was performed using RSSI (Received Signal Strength Indication), which is provided by the gateway itself with each incoming data frame. The data were transmitted from several selected locations (marked green) near the monitored ventaroles (marked blue; some of them cover 1:1) and contained directly geographical coordinates in WGS84 format, obtained by the localization of a mobile phone. The data obtained were then plotted on a map and interpolated in the QGIS geographic information system, as shown on figure 5.5.

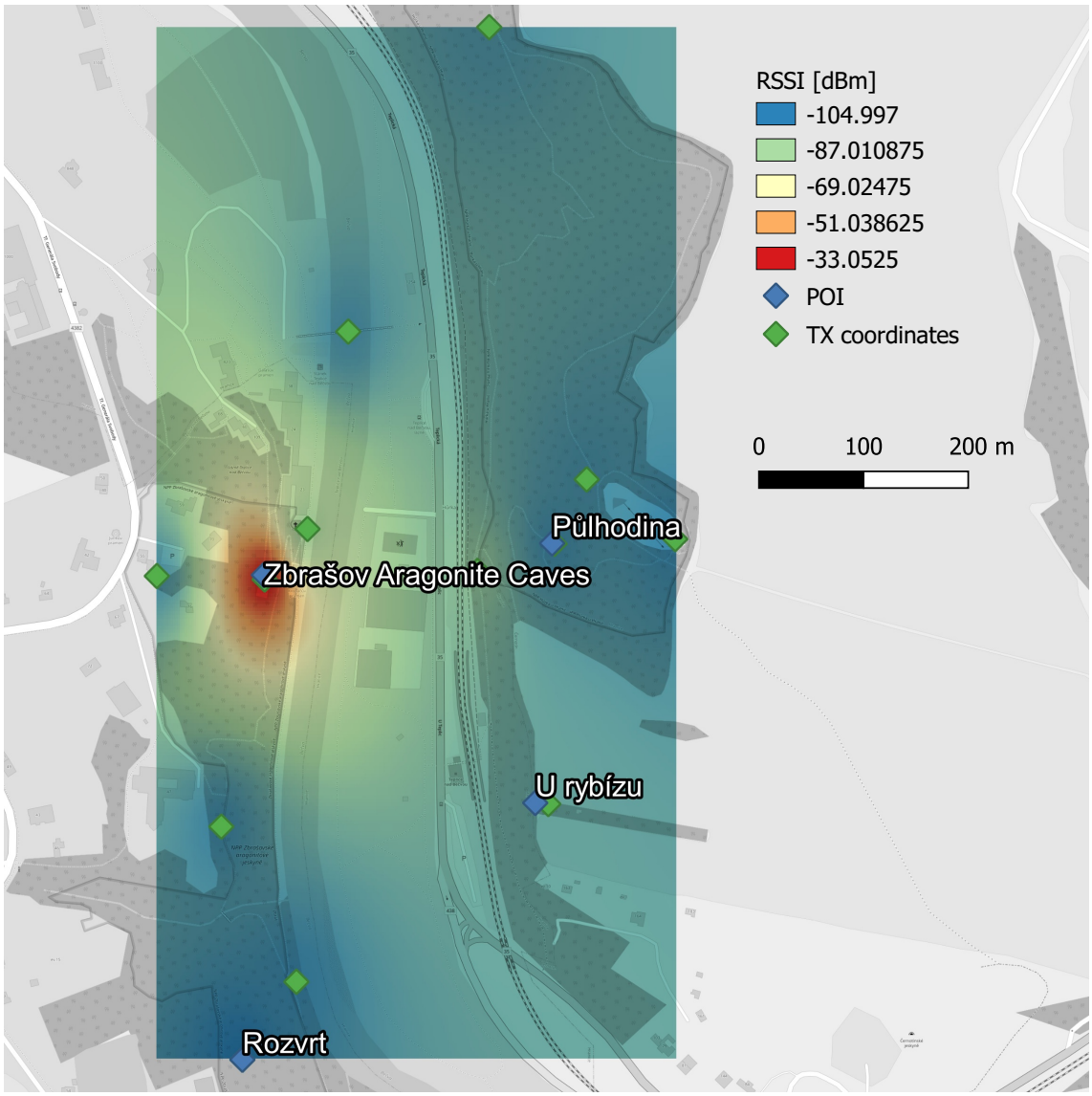

Fig. 5.2: LoRa RSSI terrain measurement results, viewed in QGIS (author)

Due to the nature of the landscape of the Bečva river valley in the area of measurement, the behavior of the transmission channel can be assumed to be well predictable.

The predictability of relatively clear transmission can be seen also on terrain profiles below, showing relatively direct point-to-point visibility. These points are ground-to-ground, without respecting for example the height of ZAC builing, antenna placement etc. Therefore images below have only illustrational character.

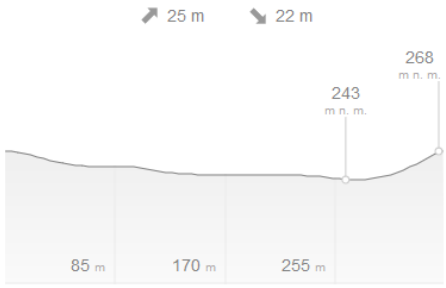

Fig. 5.3: Terrain profile between ZAC and U rybízu (author, made with and adopted from Mapy.cz)

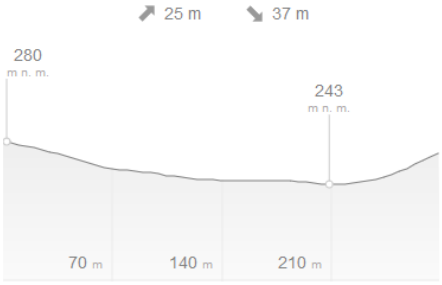

Fig. 5.4: Terrain profile between ZAC and Půlhodina (author, made with and adopted from Mapy.cz)

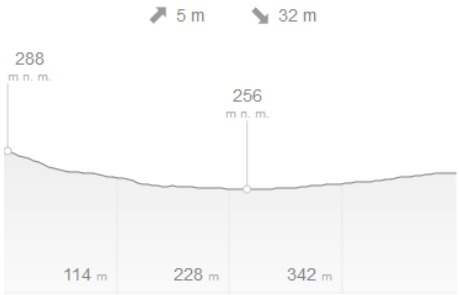

Fig. 5.5: Terrain profile between ZAC and Rozvrt (author, made with and adopted from Mapy.cz)

6 Conclusion

The main goal of this masters thesis was to design a complex field measuring network for measuring and monitoring selected environmental parameters. This was a complex problem, which included both mechanical and electronic design of device for very specific data collection and their wireless transmission, as well as design of a data concentrator for collecting the data.

For a successful path from prototype to final design it was first necessary to get acquainted with the available means of implementation and experience in the field of interest. The requirements for the measuring were then defined and a complete design of a complex system based on LoRaWAN was created.

Prototype testing provided starting points for further development iterations that converge to optimization. The functionality has been verified purely in principle, however the system appears promising in terms of usability mainly due to field experiments with signal transmission, which provided very good results.

Objectively, it is necessary to complete the program equipment to meet all the system requirements. Furthermore, it will be necessary to test the system directly in the field, which also did not happen in time. However, probably good results can be expected, thanks to the the response of the tested sensors to the measured quantities during the experiment in the room compared to previous measurements of soil CO_2 in the area in terms of sensitivity of chosen sensors.

This work primarily created a fully working infrastructure that will allow future expansion of data collection from other measurements, including improvements to existing measurements and using the third-party devices as well.

Bibliography

[1] R. Madsen, L. Xu, and D. Mcdermitt, "Considerations for making chamber-based soil co2 flux measurements," *World Congress of Soil Science: Soil Solutions for a Changing World*, vol. Congress Symposium 4 Greenhouse gases from soils, no. 19th, pp. 22–31, 1-6 August 2010. [Online]. Available: https://www.iuss.org/19th%20WCSS/Symposium/pdf/1272.pdf

[2] "Li-cor." [Online]. Available: https://www.licor.com/env/products/soil_flux/

[3] "Lorawan® specification v1.0.3." [Online]. Available: https://lora-alliance.org/resource-hub/lorawanr-specification-v103

[4] G. Gerlach, U. Guth, and W. Oelßner, *Carbon Dioxide Sensing*. Boschstr. 12, 69469 Weinheim, Germany: Wiley-VCH Verlag GmbH & Co. KGaA, 2019.

[5] "Stm32l0x0 value line." [Online]. Available: https://www.st.com/en/microcontrollers-microprocessors/stm32l0x0-value-line.html

[6] "Stmicroelectronics stm32 system-on-chip accelerates creation of smart devices with lora® iot connections." [Online]. Available: https://newsroom.st.com/media-center/press-item.html/p4208.html

[7] "Texas instrumens." [Online]. Available: http://www.ti.com/lit/ds/symlink/lm63625-q1.pdf?&ts=1589795687621

[8] "The things network." [Online]. Available: https://www.thethingsnetwork.org/

[9] "From zero to lorawan in a weekend." [Online]. Available: https://github.com/ttn-zh/ic880a-gateway/wiki

[10] J. Hromas, *Jeskyně*, vyd. 1 ed. Praha: Agentura ochrany přírody a krajiny ČR, 2009.

[11] G. Hauke, *An introduction to fluid mechanics and transport phenomena*. Dordrecht: Springer, c2008.

[12] H. Lundegardh, "Carbon dioxide evolution of soil and crop growth," *Soil Science*, vol. 23, no. 6, pp. 417–453, 1927. [Online]. Available: http://journals.lww.com/00010694-192706000-00001

[13] M. Pavelka, M. Acosta, R. Kiese, N. Altimir, C. Brümmer, P. Crill, E. Darenova, R. Fuß, B. Gielen, A. Graf, L. Klemedtsson, A. Lohila, B. Longdoz, A. Lindroth, M. Nilsson, S. M. Jiménez, L. Merbold,

L. Montagnani, M. Peichl, M. Pihlatie, J. Pumpanen, P. S. Ortiz, H. Silvennoinen, U. Skiba, P. Vestin, P. Weslien, D. Janous, and W. Kutsch, "Standardisation of chamber technique for co2, n2o and ch4 fluxes measurements from terrestrial ecosystems," *International Agrophysics*, vol. 32, no. 4, pp. 569–587, 2018-12-01. [Online]. Available: http://archive.sciendo.com/INTAG/intag.2017.32.issue-4/intag-2017-0045/intag-2017-0045.pdf

[14] S. P. Beier, *Transport Phenomena in a Physical World*, 2nd ed. On-line: Bookboon.com, 2015.

[15] Wikipedia contributors, "Venturi effect — Wikipedia, the free encyclopedia," https://en.wikipedia.org/w/index.php?title=Venturi_effect&oldid=950683048, 2020, [Online; accessed 26-May-2020].

[16] "Semtech." [Online]. Available: http://wiki.lahoud.fr/lib/exe/fetch.php?media=an1200.22.pdf

[17] "Wikipedia contributors: Spread spectrum — Wikipedia, the free encyclopedia," https://en.wikipedia.org/w/index.php?title=Spread_spectrum&oldid=946506001, 2020, [Online; accessed 26-May-2020].

[18] "Wikipedia contributors: Direct-sequence spread spectrum – Wikipedia, the free encyclopedia," https://en.wikipedia.org/w/index.php?title=Direct-sequence_spread_spectrum&oldid=954223274, 2020, [Online; accessed 26-May-2020].

[19] "Wikipedia contributors: Chirp spread spectrum – Wikipedia, the free encyclopedia," https://en.wikipedia.org/w/index.php?title=Chirp_spread_spectrum&oldid=934101195, 2020, [Online; accessed 26-May-2020].

[20] J. Welles, T. Demetriades-Shah, and D. McDermitt, "Considerations for measuring ground co2 effluxes with chambers," *Chemical Geology*, vol. 177, no. 1-2, pp. 3–13, 2001. [Online]. Available: https://linkinghub.elsevier.com/retrieve/pii/S0009254100003880

[21] "Mg811 datasheet." [Online]. Available: https://sandboxelectronics.com/files/SEN-000007/MG811.pdf

[22] "Datasheet sensirion scd30sensor module." [Online]. Available: https://www.sensirion.com/fileadmin/user_upload/customers/sensirion/Dokumente/9.5_CO2/Sensirion_CO2_Sensors_SCD30_Datasheet.pdf

[23] "Nucleo-l010rb." [Online]. Available: https://www.st.com/en/evaluation-tools/nucleo-l010rb.html

[24] “Microchip.” [Online]. Available: https://ww1.microchip.com/downloads/en/DeviceDoc/40001784B.pdf

[25] “Ebyte e32-868t20d.” [Online]. Available: http://www.ebyte.com/en/product-view-news.aspx?id=132

[26] “Stm32wl, the 1st mcu with embedded lora transceiver, a masterclass in chip design.” [Online]. Available: https://blog.st.com/stm32wl/

[27] “The things network.” [Online]. Available: https://www.thethingsnetwork.org/docs/gateways/start/build.html

[28] “Kicad eda.” [Online]. Available: https://kicad-pcb.org/

[29] “Electronic design automation consortium.” [Online]. Available: https://web.archive.org/web/20150802073506/http://www.edac.org/industry

[30] “Texas instruments: Lm63625-q1.” [Online]. Available: https://www.ti.com/product/LM63625-Q1

[31] “An4467.” [Online]. Available: www.st.com

[32] “Citizen.” [Online]. Available: http://cfd.citizen.co.jp/english/prod-tech/product/pdf/datasheet_TF/CM250C_E.pdf

[33] “On semiconductor.” [Online]. Available: https://www.onsemi.com/pub/Collateral/BSS84-D.PDF

[34] “Microchip.” [Online]. Available: http://ww1.microchip.com/downloads/en/devicedoc/50002346c.pdf

[35] “Analogdialogue.” [Online]. Available: https://www.analog.com/en/analog-dialogue/articles/how-to-control-fan-speed.html

[36] “Raspberry pi.” [Online]. Available: https://www.raspberrypi.org/

[37] “Ic880a-spi lora® concentrator.” [Online]. Available: https://wireless-solutions.de/products/lora/radio-modules/ic880a-spi/

[38] “Open iot.” [Online]. Available: https://openiot.network/

[39] “Scw12 12w dc-dc regulated single output converter.” [Online]. Available: https://www.meanwell.com/Upload/PDF/SCW12/SCW12-SPEC.PDF

[40] “Raspberry pi: Power supply.” [Online]. Available: https://www.raspberrypi.org/documentation/hardware/raspberrypi/power/README.md

[41] “Sectron ao-a868-g410s.” [Online]. Available: https://eshop.sectron.cz/cs/antena-868-mhz-stick-90-180-g410-3-dbi-sma-m-cerna/p-12703/

[42] “Raspbian downloads.” [Online]. Available: https://www.raspberrypi.org/downloads/

[43] “Libelium waspmote project.” [Online]. Available: https://github.com/avbentem/libelium-waspmote-lorawan

List of appendices

A Schematics

MCU Connections

SWD

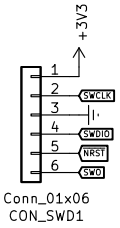

Crystals

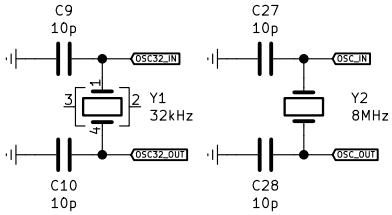

Microcontroller STM32L010RB

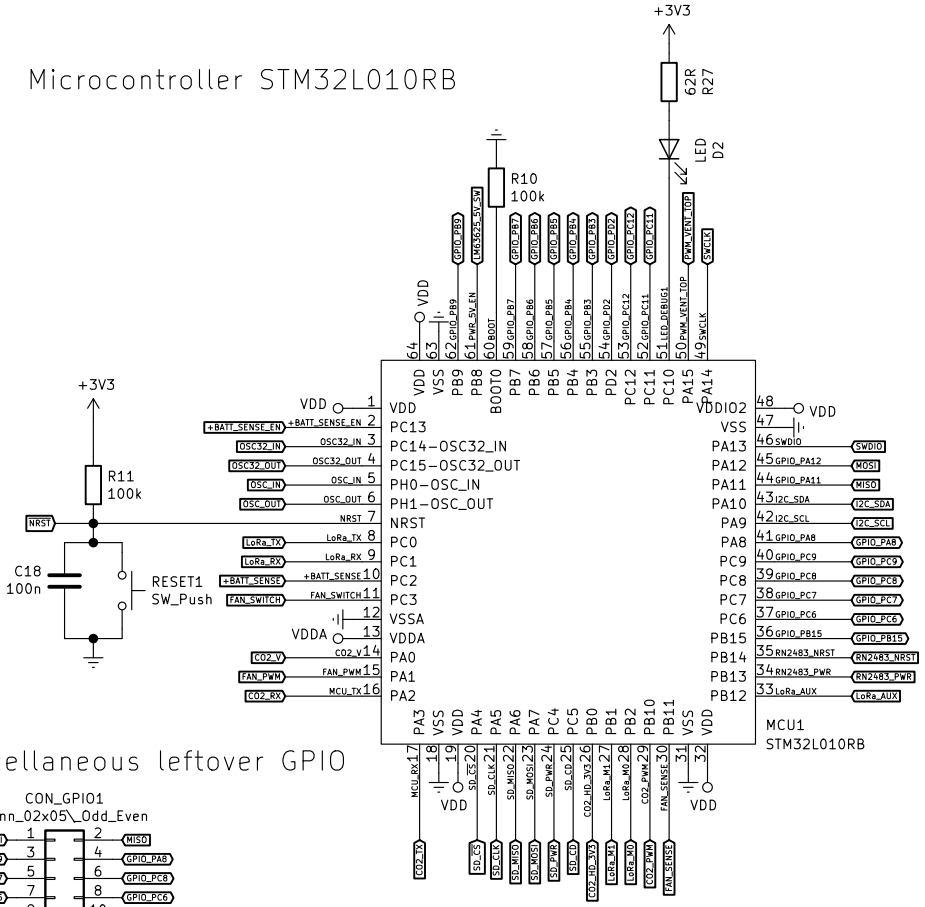

MCU power

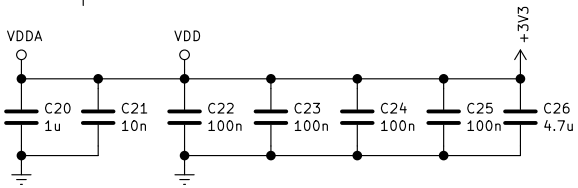

Miscellaneous leftover GPIO

Sheet: control-box-peripherals

File: control-box-peripherals.sch

Sheet: control-box-power

File: control-box-power.sch

Sheet: / File: control-box.sch		
Title:		
Size: A4	Date:	**Rev:**
KiCad E.D.A. kicad (5.1.5)-3		Id: 1/3

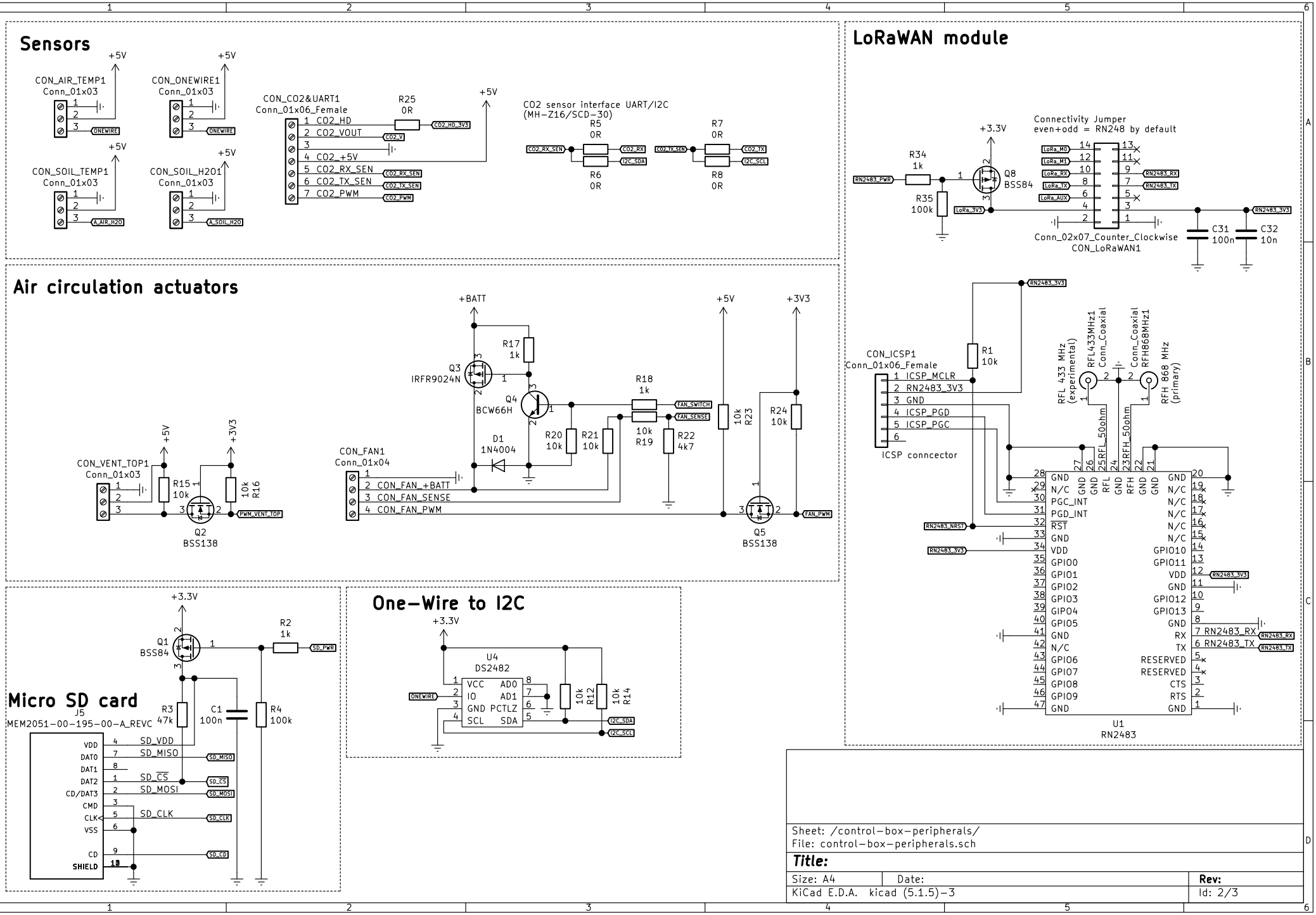
Sensors
CON_AIR_TEMP1
Conn_01x03
CON_ONEWIRE1
Conn_01x03
CON_SOIL_TEMP1
Conn_01x03
CON_SOIL_H201
Conn_01x03
CON_CO2&UART1
Conn_01x06_Female
1 CO2_HD
2 CO2_VOUT
3
4 CO2_+5V
5 CO2_RX_SEN
6 CO2_TX_SEN
7 CO2_PWM
R25
0R
CO2 sensor interface UART/I2C
(MH-Z16/SCD-30)
R5
0R
R6
0R
R7
0R
R8
0R
+5V
ONEWIRE
A_AIR_H2O
A_SOIL_H2O
CO2_HD_3V3
CO2_V
CO2_RX_SEN
CO2_TX_SEN
CO2_PWM
CO2_RX
CO2_TX
I2C_SDA
I2C_SCL
Air circulation actuators
CON_VENT_TOP1
Conn_01x03
R15
10k
R16
10k
Q2
BSS138
PWM_VENT_TOP
+BATT
+3V3
CON_FAN1
Conn_01x04
1
2 CON_FAN_+BATT
3 CON_FAN_SENSE
4 CON_FAN_PWM
Q3
IRFR9024N
Q4
BCW66H
D1
1N4004
R17
1k
R18
1k
R19
10k
R20
10k
R21
10k
R22
4k7
R23
10k
R24
10k
Q5
BSS138
FAN_SWITCH
FAN_SENSE
FAN_PWM
LoRaWAN module
Connectivity Jumper
even+odd = RN248 by default
R34
1k
R35
100k
Q8
BSS84
RN2483_PWR
LoRa_3V3
LoRa_M0
LoRa_M1
LoRa_RX
LoRa_TX
LoRa_AUX
RN2483_RX
RN2483_TX
Conn_02x07_Counter_Clockwise
CON_LoRaWAN1
C31
100n
C32
10n
RN2483_3V3
CON_ICSP1
Conn_01x06_Female
1 ICSP_MCLR
2 RN2483_3V3
3 GND
4 ICSP_PGD
5 ICSP_PGC
6
ICSP conncector
R1
10k
RFL 433 MHz
(experimental)
RFL433MHz1
Conn_Coaxial
Conn_Coaxial
RFH868MHz1
RFH 868 MHz
(primary)
RFL_50ohm
RFH_50ohm
GND
N/C
PGC_INT
PGD_INT
RST
VDD
GPIO0
GPIO1
GPIO2
GPIO3
GPIO4
GPIO5
N/C
GPIO6
GPIO7
GPIO8
GPIO9
GPIO10
GPIO11
GPIO12
GPIO13
RX
TX
RESERVED
CTS
RTS
U1
RN2483
RN2483_NRST
Micro SD card
J5
MEM2051-00-195-00-A_RECV
VDD
DAT0
DAT1
DAT2
CD/DAT3
CMD
CLK
VSS
CD
SHIELD
SD_VDD
SD_MISO
SD_CS
SD_MOSI
SD_CLK
SD_CD
Q1
BSS84
R2
1k
R3
47k
C1
100n
R4
100k
SD_PWR
One-Wire to I2C
U4
DS2482
VCC
IO
GND
SCL
AD0
AD1
PCTLZ
SDA
R12
10k
R14
10k
Sheet: /control-box-peripherals/
File: control-box-peripherals.sch
Title:
Size: A4
Date:
Rev:
KiCad E.D.A. kicad (5.1.5)-3
Id: 2/3

Power Management

Battery +12V

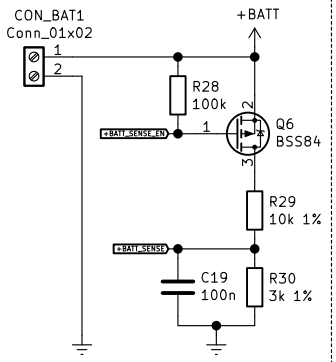

Power +3V3

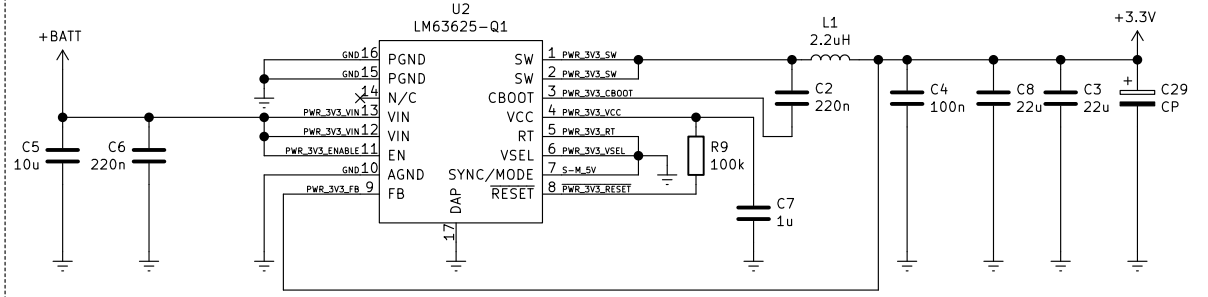

Power +5V

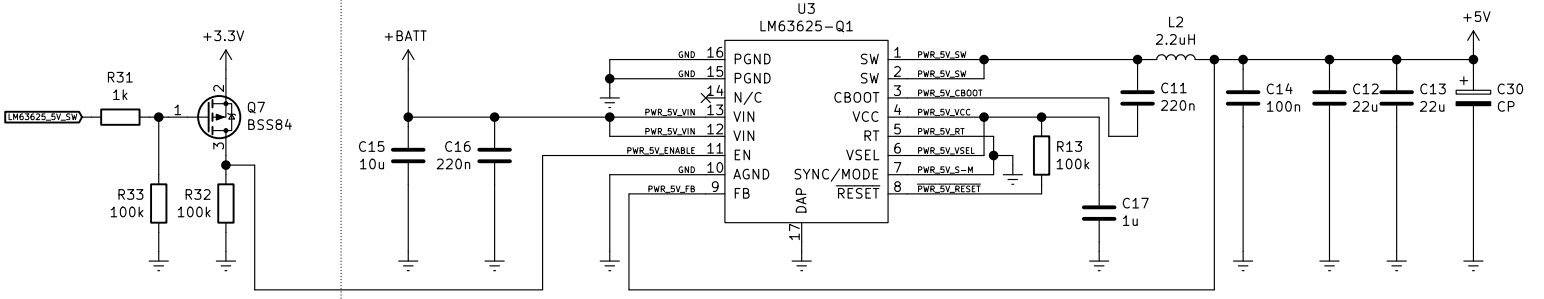

Sheet: /control-box-power/ File: control-box-power.sch		
Title:		
Size: A4	Date:	**Rev:**
KiCad E.D.A. kicad (5.1.5)-3		Id: 3/3

The "Gateway box"

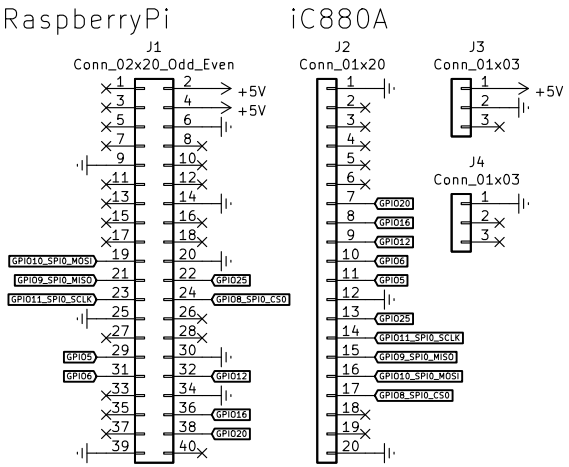

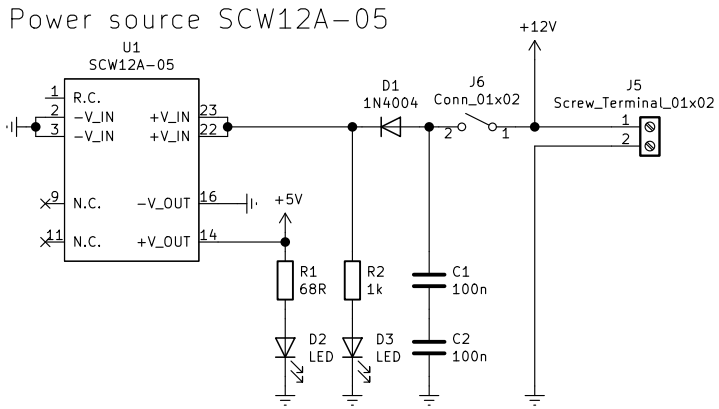

Sheet: / File: gateway-box.sch		
Title:		
Size: A4	Date:	**Rev:**
KiCad E.D.A. kicad (5.1.5)-3		Id: 1/1

B Designed hardware

B.1 Control box 3D models from KiCAD

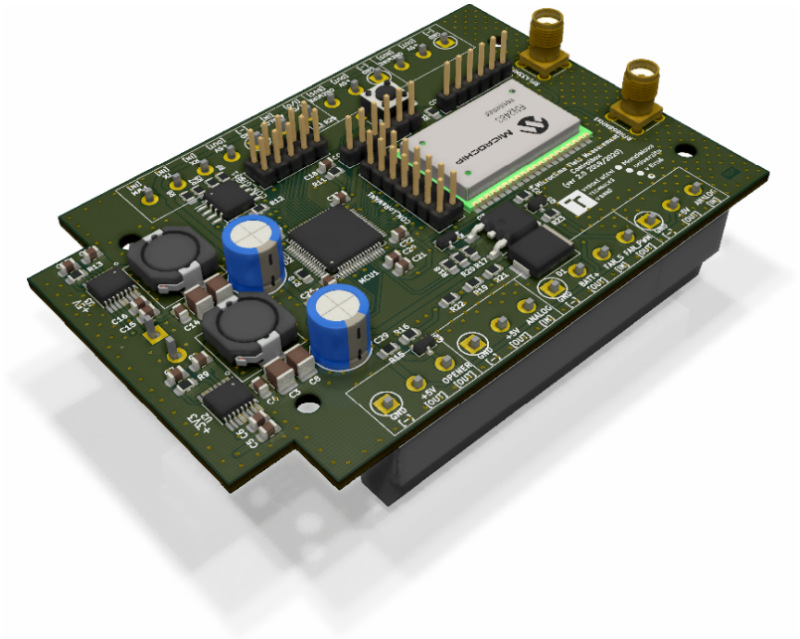

Fig. B.1: Top view of control box KiCAD 3D model (author)

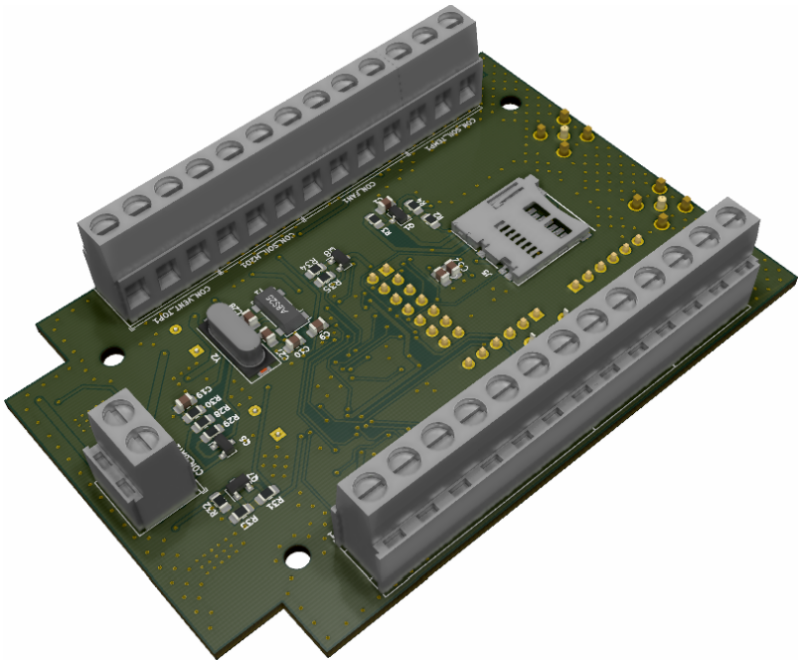

Fig. B.2: Bottom view of control box KiCAD 3D model (author)

B.2 Control box photographs

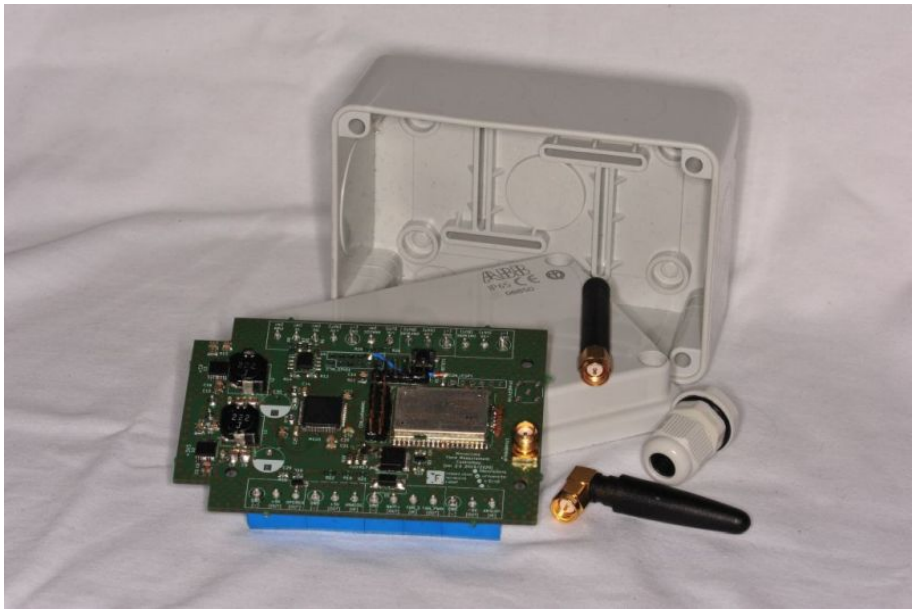

Fig. B.3: Top view of control box hardware (author)

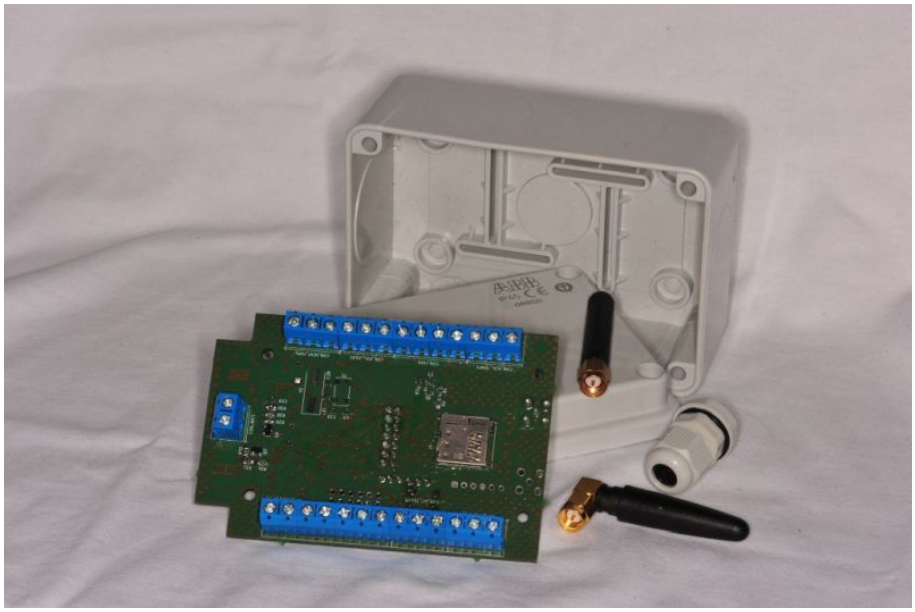

Fig. B.4: Bottom view of control box hardware (author)

B.3 Interconnecting board for the gateway

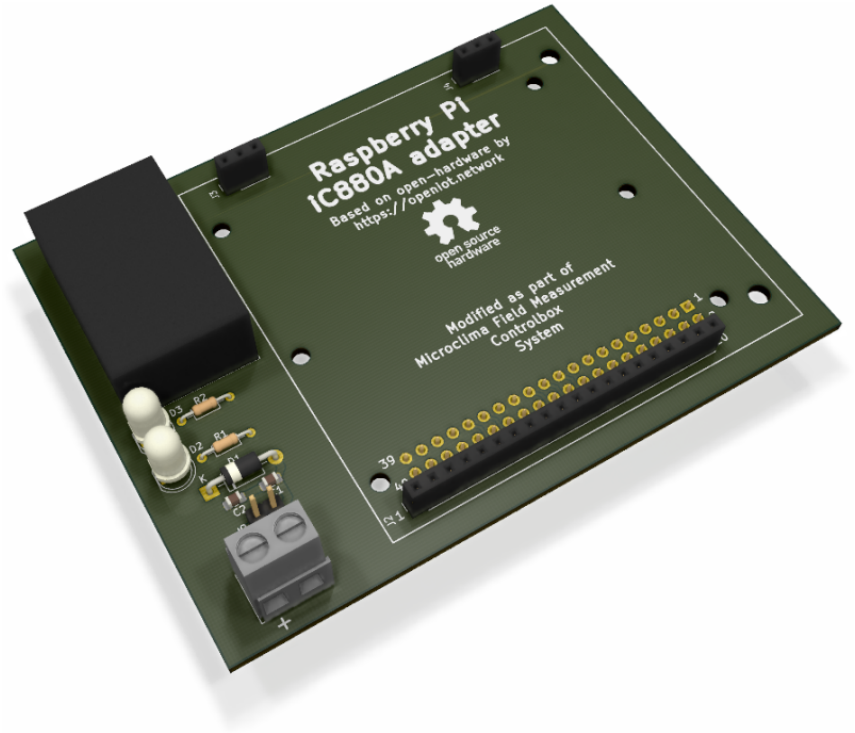

Fig. B.5: Top view of gateway interconnecting board KiCAD 3D model (author)

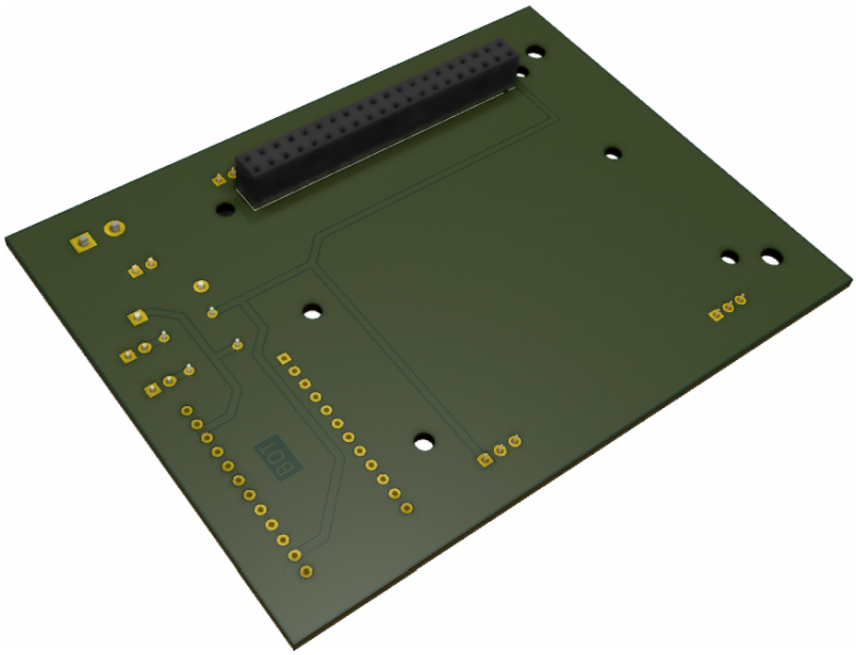

Fig. B.6: Bottom view of gateway interconnecting board KiCAD 3D model (author)

B.4 Gateway

Fig. B.7: The gateway all together (author)

C Firmware development continuum

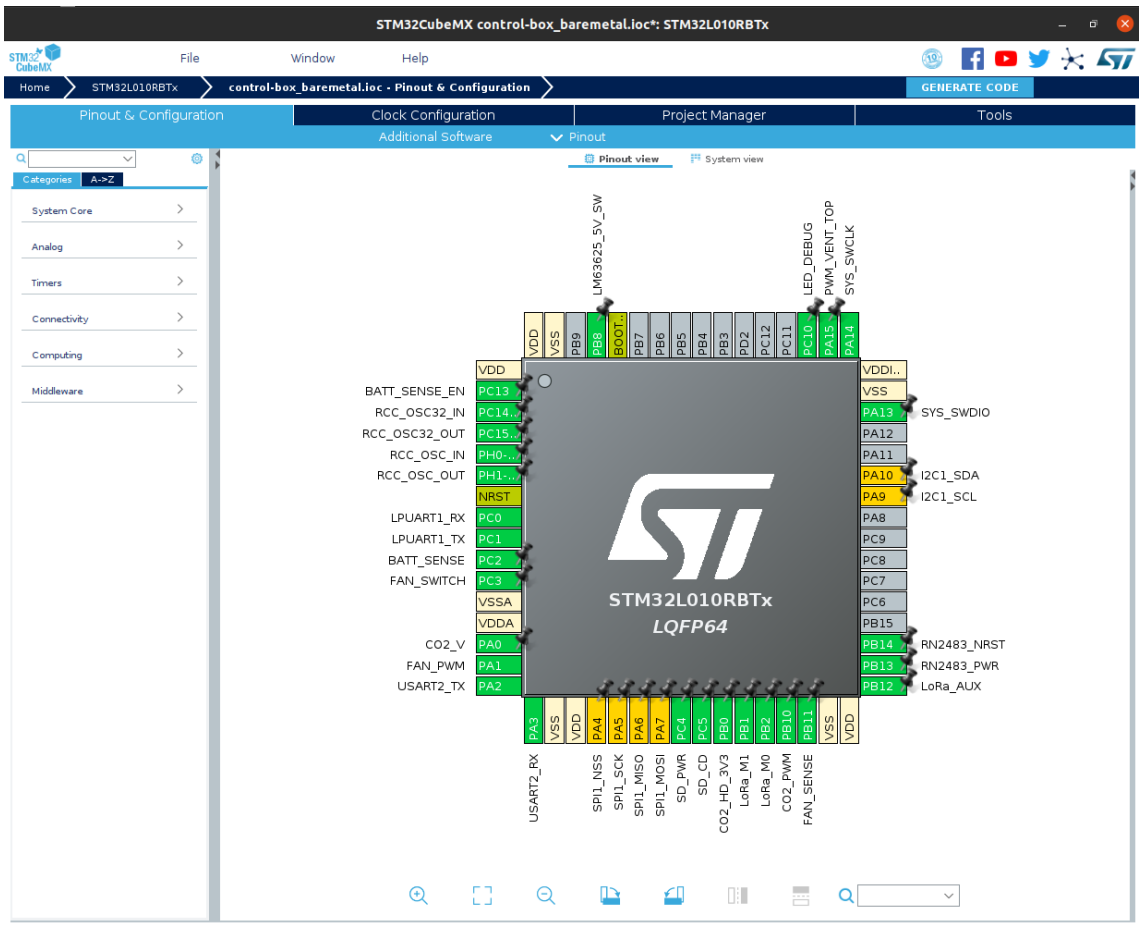

Fig. C.1: Screenshot of STM CubeMX with opened project "control-box_baremetal", Ubuntu 20.04 (author)

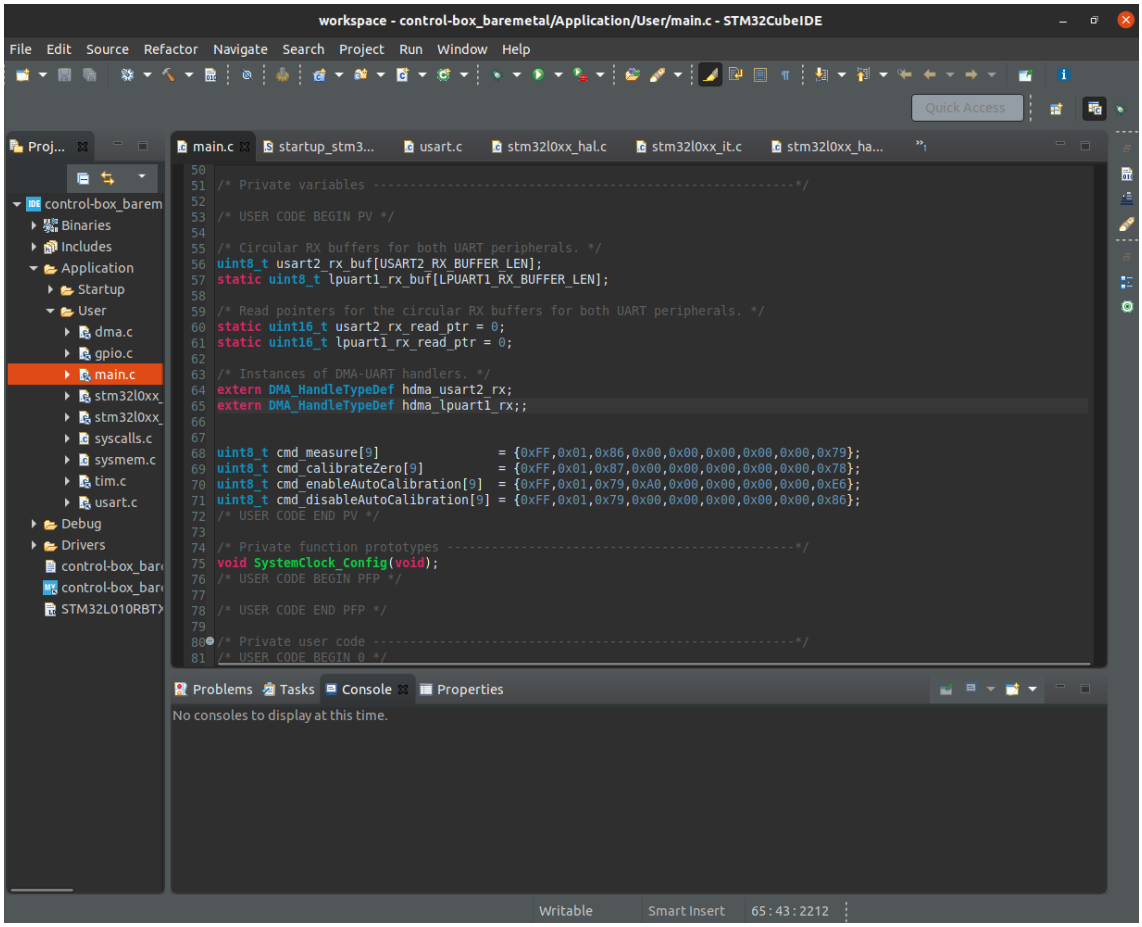

Fig. C.2: Screenshot of STM CubeIDE with opened project "control-box_baremetal", generated from CubeMX, Ubuntu 20.04 (author)

D Field experiments with LoRaWAN signal

Fig. D.1: RN2483 testing set, "Hůrka, Na rozhraní", WGS84: N 49°32.22497', E 17°44.92267' (author)

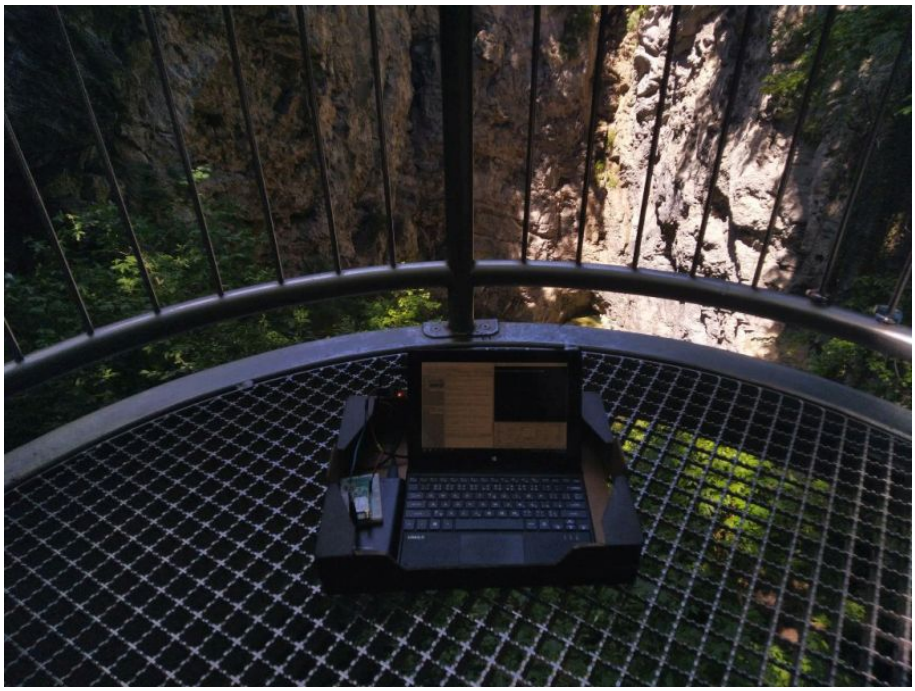

Fig. D.2: RN2483 testing set, "Hranická propast" / "Hranice abyss", WGS84: N 49°31.92217', E 17°45.07080' (author)

Fig. D.3: RN2483 testing set, "Hůrka", WGS84: N 49°31.90587', E 17°44.91427' (author)